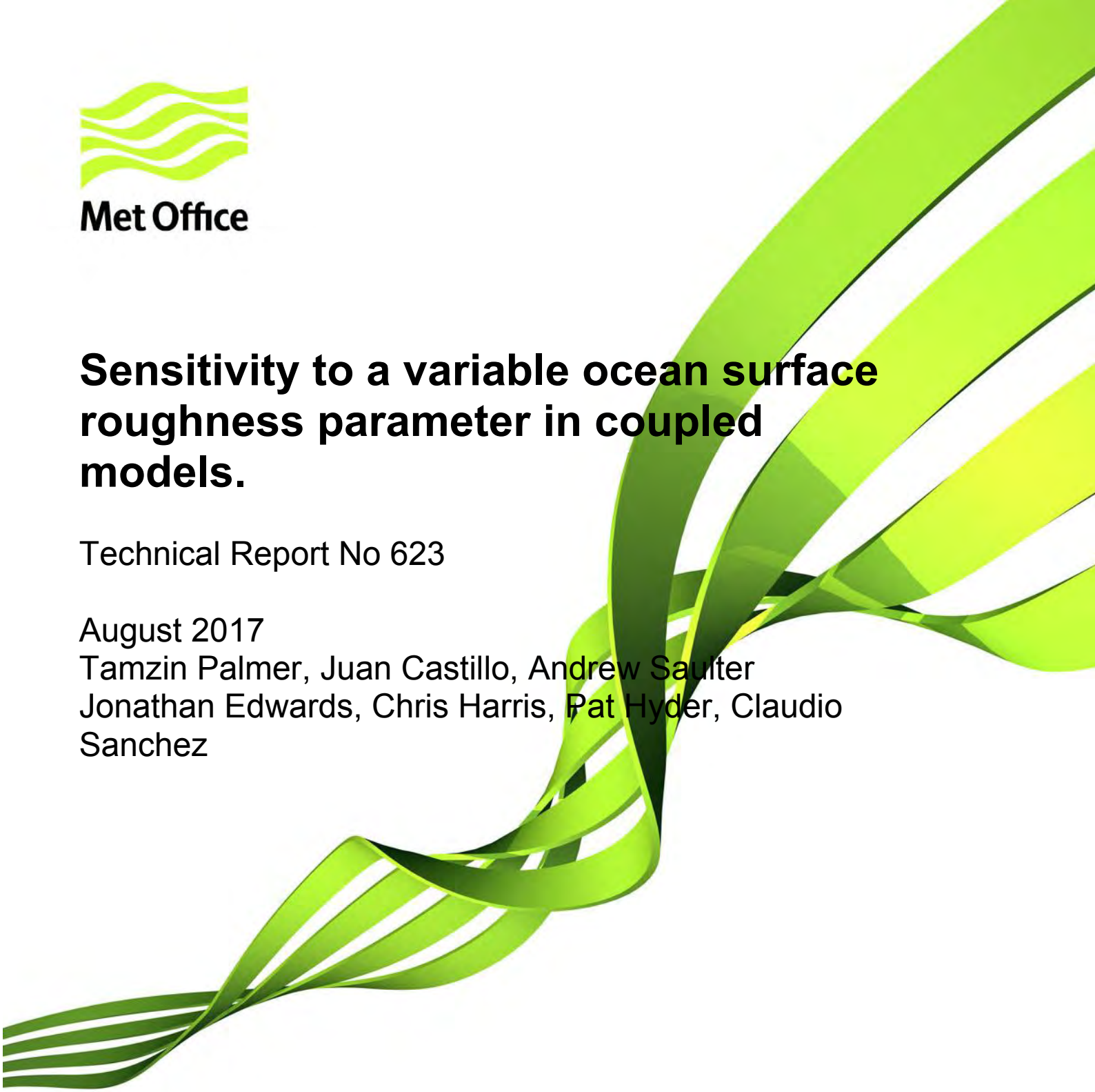

Sensitivity to a variable ocean surface roughness parameter in coupled models.

Technical Report No 623

August 2017

Tamzin Palmer, Juan Castillo, Andrew Saulter
Jonathan Edwards, Chris Harris, Pat Hyder, Claudio Sanchez

Contents

EXECUTIVE SUMMARY **3**

1. Introduction **5**

1.1 Motivation for sensitivity study 5

1.2 Momentum fluxes in the coupled ocean and atmosphere model 5

1.3 Sea Surface Roughness: specification by wave models 6
1.3.1 Previous literature for atmosphere-wave coupling 6
1.3.2 Coupling using a variable Charnock parameter 9

1.4 Sensitivity Tests 10

2. Methodology **12**

2.1 Coupled and atmosphere only models. **12**

2.2 Models 13
2.2.1 The Global Coupled Model 2.0 13
2.2.2 Met Office Unified Model Global Atmosphere 6.0 13
2.2.3 Global Ocean Model 5.0 14
2.3.4 Wave Model 15

3. Results **19**

3.1 The Wave Growth and Dissipation Terms in a Single Point Model. 19
3.2.1 Patterns in Charnock parameter 25
3.2.2 Changes in the Scalar 10m wind speed. 30

3.3 Wave Coupling Impacts on Storm Tracks. 34

3.4 Precipitation sensitivities to wave coupling 38

4. Ocean-Wave Atmosphere coupling sensitivities **40**

4.1 Charnock Patterns 40

4.2 Precipitation and 10m Scalar Winds 40

4.2 Sea Surface Temperature and salinity 44

4.3 Heat Fluxes 47

5. Discussion **50**

5.1 ST3 and ST4 source terms **50**

5.2 Regional sensitivity **51**

5.3 Sensitivities of ocean feedbacks to atmosphere-wave coupling. **51**

5.4 Performance of the atmosphere-wave coupled models. 53

6. Conclusions **55**

6.1 Summary and Conclusions **55**

6.2 Recommendations for future work 56

7 References **57**

8 Appendix **60**

8.1 Changes in wind stress 60

8.2 Changes in Pressure at mean sea level. 62

8.3 Geopotential Height 64

8.4 Wind speed errors compared to climatology 66

8.5 Heat flux changes for AW-ST4 67

EXECUTIVE SUMMARY

The sensitivity of the GA6.0 Met Office atmosphere model and the GC2 atmosphere-ocean coupled model to a sea state dependent Charnock parameter was tested in a set of 20 year climate experiments. An (approx. 60km horizontal resolution) atmosphere model was coupled to a global, 50km resolution, WAVEWATCH III (v4.18) model. In the first two experiments wave and atmosphere models were coupled via a variable Charnock parameter. This influenced the roughness length and the drag coefficient in the atmosphere model over the ocean surface. The two experiments used two different sets of wave model source terms, following WAM cycle 4 (Komen, 1994; Bidlot et al. 2012) and Ardhuin et al. (2010), resulting in different Charnock values being passed to the atmosphere model. In the third experiment the wave model and atmosphere model were again coupled using a variable Charnock parameter. The atmosphere and ocean model were fully coupled to exchange heat, moisture, freshwater and momentum fluxes. The ocean and waves were not directly coupled; therefore the waves only influenced the ocean via changes in the atmosphere model.

The largest sensitivity to the atmospheric model coupling with the wave model was seen in the 10m scalar wind speeds, in particular in the North Atlantic storm belt. These changes were not unexpected as the Charnock coefficient affects the drag coefficient of the winds over the ocean this turn affects the wind speeds. However, some sensitivity to the coupling was also seen throughout the atmosphere column and in the heat fluxes. There were also potentially significant changes in the evaporation and precipitation that were related to changes in the wind speed and the location of the main storm belts. An analysis of the known Gulf Stream storm genesis region showed some quite subtle changes between the runs but suggested that feedbacks between the models in this area could be important. The different wave model source terms produced different Charnock values. The values produced using the WAM cycle 4 terms (Komen, 1994; Bidlot et al. 2012) were generally lower but also had a greater variability that those produced by the source terms of Ardhuin et al. (2010).

The addition of the ocean model in the form of the GC2 atmosphere-ocean coupled model introduced further sensitivities, due to the strength of the feedback from the ocean to changes in the atmosphere. The changes in the 10m wind speeds were different in the case of the ocean-atmosphere-wave coupling. These changes were most significant in the North Atlantic where in some parts an increase in wind speed occurred in the

winter months, where it had decreased in the wave-atmosphere coupled experiments. The changes introduced by using the wave model based surface roughness, led to complex feedbacks that also affected the sensitive and latent heat flux in the North Atlantic. The mixed layer depth also increased significantly in parts of the North Atlantic in response to changes in the wind speed.

Recommendations for future work include direct coupling between the wave and the ocean model. It may also be useful to investigate the use of a variable Charnock parameter in a short range coupled forecast that is constrained by data assimilation.

1. Introduction

1.1 Motivation for sensitivity study

Coupling between atmosphere and ocean models is used to improve the performance of both models though the exchange of heat, moisture, freshwater and momentum fluxes. Component models have poor representation of the surface boundary condition which leads to errors.

The European Centre for Medium Range Weather Forecasting (ECMWF) has coupled its wave and atmosphere model for over 15 years. Published literature shows (e.g. Janssen 2001) that the exchange of surface roughness information in the form of the Charnock parameter between the wave and the atmosphere has led to an improvement in the performance of both the models. The purpose of this study is to establish the potential sensitivity of the Met Office atmosphere and ocean model to coupling with the Met Office wave model via the exchange of the Charnock parameter. This is a first step towards scoping the coupling of the atmosphere and wave model on a global scale.

1.2 Momentum fluxes in the coupled ocean and atmosphere model

The ocean-ice system and atmosphere communicate via heat, moisture, freshwater, momentum and gas/particle fluxes. The temporal evolution of these exchanges involved a myriad of complex coupled processes. For example, local sea-surface temperatures (SSTs) and ocean currents influence fluxes of heat and moisture to the atmosphere; these in turn influence the atmospheric boundary layer structure, including its temperature and humidity that control its density and associated convection and upper atmosphere heating when moisture condenses (Roberts et al. 2016, Chelton and Xie 2010). In turn this can influence the density gradients and associated baroclinicity of the atmosphere, and hence the lateral transports and characteristics of storms. This effect is particularly pronounced over ocean boundary and frontal currents, where SST gradients cause very large heat and moisture fluxes that can influence the atmosphere right up to the tropopause (Minobe et al. 2008). At the same time; local atmospheric clouds (and aerosols or moisture), winds, near surface humidity, air temperature and rain, influence surface heat, freshwater and momentum fluxes to the ocean. This changes local temperature and salinity and hence density, thus changing ocean lateral and vertical heat and salt transports, including ocean convection. In addition, non-local impacts of

these coupling sensitivities affect atmospheric and oceanic density gradients that influence lateral and vertical heat transports and atmospheric and oceanic states.

Within this system, waves affect the roughness of the ocean surface or drag on the overlying atmosphere. This impacts on the vertical structure of near-surface winds within the atmospheric boundary layer and associated wind stress (i.e. the rate of momentum transfer). In turn, this affects the transfer of moisture, heat and particles across the surface.

When a coupled model is initiated from a realistic state, drifts and biases evolve simultaneously in all of these coupled interactions. This makes it extremely difficult to understand causes of coupled evolving biases. In models without coupling the effect of roughness is to some degree represented, based on local winds by empirically derived transfer coefficients (which represent a local sea at a fixed stage of development). However, since these parameterizations have no knowledge of sea-state they cannot represent young seas or swell wave effects. Hence, including a wave model in the coupled configuration offers the potential to better represent ocean surface roughness and associated drag on the atmosphere.

From the wave model viewpoint, the key uncertainties affecting surface roughness are the atmospheric forcing and the source terms used to describe wave growth and dissipation. For this reason, to try to understand the coupled sensitivities to any model it is extremely helpful to consider the different sensitivities of the wave model to different source term physics in isolation.

1.3 Sea Surface Roughness: specification by wave models

1.3.1 Previous literature for atmosphere-wave coupling

Wind generated ocean waves form the boundary between the atmosphere and the ocean. The sea-state in this boundary layer is known to have an important influence on the air-sea momentum transfer (Janssen 1989, Janssen et al., 2001).

The presence of waves on the ocean surface increases the surface drag and momentum transfer from the wind to the waves affects the atmospheric boundary layer (Cavaleri et al., 2012). In particular, the interaction between the waves and the atmospheric

boundary layer will affect storm development. The enhanced surface drag from the waves has the effect of reducing the wind-speed; this effect is greater in regions of young wind-seas. As the wind blows over the ocean surface, capillary waves develop, increasing the roughness of the surface. The wind transfers momentum to the waves causing them to grow in size. In the early stages of the development of the waves, the sea state is fairly chaotic with a broad directional spread. These young sea states result in the ocean taking up a larger proportion of momentum from the atmosphere. As the wind continues to blow the waves become larger and less steep resulting in a reduction of the drag. Experimental evidence has shown that the drag coefficient may vary by a factor of 2 between young and old wind-sea (Janssen et al. 2001).

There are a number of approaches to defining the surface roughness(e.g. Taylor and Yelland, 2001, Drennan et al., 2003); however the most widely used is the Charnock parameter (α_{CH}). In this approach changes to the momentum from the atmosphere to the ocean surface are calculated as a function of the friction velocity; gravity and α_{CH} (see equation 2 in section 1.3.2). In an uncoupled atmosphere model, α_{CH} will take a constant value of typically between 0.011 and 0.018. However, the Charnock 'constant' has long been considered in the literature (e.g. Janssen 1989, 1995, and 2001) to not in fact have a constant value, but to vary with the sea-state. The sea-state will vary not only with atmospheric conditions, but also has geographic variations due to different fetch conditions throughout the global oceans. Janssen, (1989) parameterized a variable α_{CH} value based on the wave-induced stress (see equation 3). This is given as a function of the wave input source term (S_{in}), which is in turn a function of the wind speed, the underlying wave spectrum and the water density. A variable α_{CH} results in a feed back effect between the ocean surface and the 10m wind speed. As the wind speed increases the sea state starts to develop, this increases the roughness of the surface and therefore the value of α_{CH} as more momentum is transferred from the atmosphere to the waves. This in turn reduces the wind speed. As the sea-state develops and becomes smoother the wave supported stress is reduced, this begins to decrease theCharnock value. In principle the reduced surface roughness would allow faster wind speeds, as less momentum from the atmosphere is transferred to the waves. The effect on the atmospheric model of the wave coupling will depend on the value of the Charnock constant in the uncoupled model. In this case it is set to 0.018, which is higher than the global average of the Charnock value in the coupled models.

Using a variable Charnock parameter to take the wave-induced drag into account, the ECMWF (European Centre for Medium-Range Weather Forecasts) studies found a

significant impact on the synoptic pressure and wind patterns in the Southern Ocean (Janssen et al., 2001). The storm belt in this region was shifted about 10° towards the equator. The influence of waves in this region within the atmospheric model is to weaken the pressure minima and reduce the surface winds. Large biases are often present in these winds in General Circulation Models (GCMs) and these impact on the uptake of heat and CO_2 from the ocean (Cavaleri et al., 2012).

In the ECMWF study, using a sea-state dependant Charnock parameter to calculate the surface roughness was found not only to affect the 10m wind speeds and the growth of the wave spectrum. Impacts of coupling were found throughout the whole atmosphere column (Janssen and Viterbo, 1996). When comparing runs, significant differences in the wave field, surface stress, geopotential height (500 and 1000mb), temperature and rainfall were found between the coupled runs and the control.

Changes in the geopotential height were largely found to be favourable. There were also changes in the blocking frequency in the North Pacific, which were unfavourable. The largest changes were seen in the storm track regions of the North Atlantic and the Southern Ocean. In the North Atlantic the storm track was shifted south compared to the control run, the latitude of the southern hemisphere storm track also became more variable. A notable reduction occurred in the surface winds of the Southern Ocean, this was considered favourable due to a positive bias existing at the time in the 10 day ECMWF forecast. This reduction of the Southern Ocean wind speeds was related to the weakening of surface pressure lows due to the increased roughness of the young wind-seas.

Recent studies by Shimura et al., (2017) also find that the surface roughness (defined by the sea-state) has a significant effect on the bulk momentum transfer coefficients. This study also observed that changes in the surface roughness affected the atmospheric model throughout the whole atmospheric column. Large-scale effects on the atmospheric circulation were also noted, in particular the Hadley circulation and corresponding changes in the precipitation of 2mm/day from the seasonal average. The differences in the surface roughness led to 1m/s changes in the surface wind climatology and the enhancement of wind speeds at low latitudes of up to 15%. Overall, when compared to observations, the surface wind speeds at low latitudes were improved, while they were over estimated at high latitudes. The impact of swell on the surface roughness was found to be very different to that of a young wind-sea; the conclusion of

this study was that further research on the interaction of swell with the atmospheric boundary layer is needed.

1.3.2 Coupling using a variable Charnock parameter

A variable Charnock field can be generated using a wave model, which is forced by the 10m wind field (U_{10}) from an atmospheric model; this is then passed to the atmospheric model and is used to recalculate the drag coefficient. This approach is similar to the early form of wave-atmosphere coupling first used by ECMWF in the 1990's (Janssen 1989).

The air side friction velocity (U_*) can be defined as (Breivik et al., 2015):

$$\boldsymbol{U_*^2 = \tau_a \rho_a = \tau} \qquad (1)$$

Where τ_a is the total air-side stress and ρ_a is the air density (a constant in this case). Charnock (1955) related the roughness of the sea surface (z_0) to the friction velocity as:

$$\boldsymbol{z_0 = \alpha_{CH} \frac{U_*^2}{g}} \qquad (2)$$

Where α_{CH} is known as the Charnock constant and g refers to the acceleration due to gravity. Janssen (1989, 1991) assumed that the Charnock parameter was not in fact constant but may vary with the sea-state.

In WAVEWATCH III a variable Charnock field can be output and the roughness modified by the wave supported stress is given as (Breivik et al., 2015):

$$\alpha_{CH} = \frac{\hat{\alpha}}{\sqrt{1-\tau_{in}/\tau_a}} \qquad (3)$$

The Charnock value calculated by the wave model is therefore largely dependant on the ratio of the air-side to wave supported stress. Note that in periods of very low winds when the wave supported stress is 0 the value of the Charnock value will default to the value of $\hat{\alpha}$ which is given as 0.006 by Bidlot (2012) and 0.01 for Ardhuin et al. (2010).

The wave supported stress τ_{in} is related to the wind input and to the wave field as (Breivik et al., 2015):

$$\tau_{in} = \rho_w g \int_0^{2\pi} \int_0^{\infty} \frac{k}{\omega} S_{in} \, d\omega d\theta \qquad (4)$$

Here ρ_w is the water density, S_{in} is the wind input source term of the wave model, k is the wave number and ω the angular frequency. The S_{in} term is described further in section 2.3.4; the wave-supported stress is essentially the integrated energy in frequency and direction of the S_{in} source term as calculated by the wave model. The air-side stress is determined from the friction velocity U_*, which is calculated from an assumed wind speed profile. Therefore the Charnock parameter, as calculated by the wave model, will change according to the S_{in} source term as the ratio of the wave induced to air-side stress changes.

The Charnock field is then passed from the wave model to the atmosphere model where it is used to calculate a new momentum roughness length as detailed in Lock et al. (2017):

$$z_{0(sea)} = \frac{1.54 \times 10^{-6}}{u_*} + \frac{\alpha}{g} u_*^2 \qquad (5)$$

It should be noted that the U_* used by the wave model will be calculated from the 10m wind speed (U_{10}) assuming a logarithmic profile. This may not correspond exactly to the value of U_* used in the atmosphere model as only the values U_{10} and α are directly exchanged. The new roughness length calculated in the model will then be used to calculated the drag coefficient over the ocean and it is this (rather than the Charnock parameter directly) that specifies the exchanged of momentum from the atmosphere to the ocean surface. The second part of the equation has a much larger impact on the value of z_0 than the first part. Therefore the changes in Charnock past to the atmosphere model will have a significant impact on the calculation of the roughness length over the ocean in the UM model.

1.4 Sensitivity Tests

The sensitivity of global coupled systems is difficult to establish due to the two way feedbacks between the atmosphere ocean and wave models. To address this difficulty, a number of simpler experiments have also been carried out to better understand the processes affecting the results.

Two atmosphere-wave 20 year climate runs to test the ST3 and ST4 wave model source terms. These are referred to in this report as AW-ST3 and AW-ST4 respectively. The AW runs were compared to the same 20 year period from a control atmospheric model run, referred to hereafter as ATM.

A 20 year atmosphere-wave-ocean coupled run is compared with 20 years of an atmosphere-ocean run. These are referred to as AOW and AO respectively. The details of the model code base and the configurations that were used are given in the following section.

2. Methodology

2.1 Coupled and atmosphere only models.

Table 1. Summary of modelling experiments.

Experiment name	Atmosphere component	Wave component	Ocean component	Control experiment
AW-ST3	UM v10.3	WAVEWATCH III v4.18 (WAM 4 source terms)	Climatology	ATM (AMIP run)
AW-ST4	UM v10.3	WAVEWATCH III v4.18 (Ardhuin et al., 2010 source terms)	Climatology	ATM (AMIP run)
AOW (ST4)	UM v10.3	WAVEWATCH III v4.18 (Arhuin et al., 2010 source terms)	NEMO v3.4	AO (GC2 coupled model)

An atmosphere only (hereafter ATM) run from the Atmospheric Intercomparison Project (AMIP) was used as a control for the sensitivity studies. The run was selected so that all aspects of the atmosphere model were the same as those used for the atmosphere-wave runs (hereafter AW-ST3 and AW-ST4). The AMIP simulations were carried out using common boundary conditions and radiative forcings. Boundary conditions were from 120 monthly observed distributions of SST's and sea ice extents from in-situ, climatological and satellite data compiled by NOAA (National Oceanic and Atmospheric Agency). This was supposed to represent a 'perfect' ocean for the purposes of the experiment. Identical specifications of the solar constant (1365W/m2) were used and the atmospheric CO2 had a concentration of 345ppm. The ocean surface currents were assumed to be zero. In the coupled run the Charnock field was exchanged between the wave model and the atmosphere at 3 hourly intervals.

The ocean-atmosphere control run used the Met Office Global Coupled Model 2.0. This is described in further detail in the following section. The coupling fields are handled and interpolated by the OASIS3-MCT coupler which exchanges momentum, freshwater and the heat flux from the atmosphere to the ocean. The surface velocity and sea ice are exchanged from the ocean to the atmosphere.

The ocean model was initialised by a climatological dataset from 2004-2008 and a 20 year sea ice mean from HadGEM1 (Hadley Centre Global Environmental Model). The coupled atmosphere-wave-ocean run was allowed a 10 year spin up period.

Three experimental global climate runs were carried out as summarised in table 1 above.

- Atmosphere wave model coupling 20 year run using WAM 4 source terms (Janssen 1991, Komen et al., 1994, Bidlot et al., 2012).
- Atmosphere wave model coupling 20 year run using source terms of Ardhuin et al. (2010).
- Atmosphere-ocean coupled model, coupled to the wave model via a Charnock parameter exchange with the atmosphere model only. The momentum transfer from the waves is not closed in this study as the wave model is not directly coupled to the ocean model. A 20 year run (with a 10 year spin up) of this coupled system was carried out. The wave model used the source terms of Ardhuin et al. (2010).

2.2 Models

2.2.1 The Global Coupled Model 2.0

The global coupled configuration of the Met Office Unified Model (UM) 2.0 (GC2) was used to test the sensitivity of the GC Met Office models to coupling with WAVEWATCH III and the atmosphere via a sea state dependent Charnock parameter. The GC2 configuration was released in March 2014 (a full description is given by Williams et al., 2015). The model is comprised of the component models; Global Atmosphere 6.0 (GA 6.0), Global Land 6.0 (GL 6.0), Global Ocean 5.0 (GO 5.0) and Global Sea Ice 6.0 (GSI 6.0); GA 6.0 and GL 6.0 are documented by Walters et al. (2015) and GO 5.0 is described by Megann et al. (2014).

2.2.2 Met Office Unified Model Global Atmosphere 6.0

The GA6.0 can be run over a wide range of horizontal resolutions on a regular latitude-longitude grid (Williams et al., 2015). In this study a horizontal resolution of N216 (about 60km at mid-latitudes) was used. The model has 85 vertical levels, 50 levels below 18km and 35 levels above.

At the heart of the model is the dynamical core which solves the equations of motion; the implementation in GA6.0 is ENDGame (Even Newer Dynamics for General atmospheric modelling of the environment; Wood et al., 2014).

The atmosphere model comprises of 3D wind, virtual dry potential pressure and dry density. These are discretized horizontally onto a regular latitude-longitude grid with Arakawa E grid staggering and vertical discretization that uses Charney-Phillips staggering. The discretized equations are solved using a nested iterative approach centred about solving a Helmholtz equation. The physical parameterizations are split into slow processes (radiation, large-scale precipitation and gravity wave drag) and fast processes (atmospheric boundary layer, turbulence, convection and land surface coupling). The slow processes are treated in parallel and computed once per time step. The source terms from the slow processes are added to the appropriate fields before interpolation. The fast processes are treated sequentially and computed using the latest predicted estimate for the required variables at the next time step.

2.2.3 Global Ocean Model 5.0

The GO5.0 model was developed jointly by the NOC (National Oceanography Centre) and the Met Office as part of the Joint Ocean Modelling Program (JOMP). The ocean model consists of NEMO v3.4 (Nucleus for European Models of the Ocean; Madec 2008).

The horizontal grid (ORCA025) has a 1/4° resolution. There is an isotropic Mercator grid in the southern hemisphere, matched by a quasi-isotropic bi-polar grid in the north hemisphere with poles at 107°W and 73°E. The grid resolution at the equator is about 26km and this increases with latitude to approximately 14km at 60° north and south.

The model has 75 vertical levels; each level thickness is a double tanh function of depth. The levels vary in thickness from 1m at the surface to 200m at 6000m. These levels were chosen to allow a high resolution at the surface for short to mid-range forecasting, while also giving a reasonable resolution at mid-depths for long-term climate studies. The bathymetry is based on the ETOPO1 dataset with additional data in coastal regions from GEBCO (General Bathymetric Chart of the Oceans).

The model has a linear free surface and an energy enstrophy conserving momentum advection scheme. The horizontal viscosity is bi-Laplacian and given a value of 1.5 x $10^{11}m^4s^{-1}$ at the equator; which reduces polewards. The tracer advection scheme uses a total variance dissipation (TVD) scheme described in Zalesak (1979). Lateral tracer mixing is along isoneutral surfaces with a coefficient of $300m^2s^{-1}$.

In the diapycnal mixing scheme, the mixing of tracers and momentum uses a modified version of Gaspar et al. (1990) turbulent kinetic energy (TKE) scheme. This is described in Madec (2008). The unresolved vertical mixing is represented by a background vertical eddy diffusivity coefficient. The bottom friction is quadratic and has an increased coefficient for the Indonesian Through flow, Denmark Strait and Bab al Mandab regions. An advection and diffusive bottom boundary scheme is included. The tidal mixing follows Simmons et al. (2004). A climatological geothermal flux term has also been included (Stein & Stein 1992).

2.3.4 Wave Model

The Met Office has used the WAVEWATCH III ocean surface model for all its operational model configurations since 2008. It is a community model initially developed by Hendrik Tolman (Tolman, 1991) and now under continual development by the wave modelling community. The operational wave model is run at the Met Office at a range of resolutions; the highest is 4km for the UK configuration, the global model is run on a variable resolution Spherical Multiple Cell (SMC) grid of 6-25km. The operational Met Office version of the model operates a second-order advection scheme (Li, 2008). The Discrete Interaction Approximation (DIA, following Hasselmann et al., 1985) is used to describe the non-linear wave-wave interactions, which redistribute the spectral energy and determine the evolution of the wave spectrum. The deep-water source term physics used for growth (wind input term) and dissipation of wave energy in the spectrum is under regular review for the operational model as the science progresses. For this study version 4.18 of the model (Tolman et al., 2014) was used. A global SMC grid was used for this study with a resolution of 50km. Two different source term physics were used for coupling with the atmosphere; these are described briefly in the following sections.

2.3.4.1 WAM Cycle 4 source terms (ST3)

The ST3 wind-wave interaction source term is based on the wave growth theory of Miles (1957), modified by Janssen (1982). The wind input term is parameterized following Janssen (1991). The implementation in WAVEWATCH III for this study used the approach of Bidlot et al. (2012). Full details of the source term are given in Tolman et al. (2014).

The wind input term is as follows:

$$S_{in} = \gamma N \qquad (6)$$

Where γ is the growth rate and N is the action density spectrum.

$$\frac{\gamma}{\omega} = \varepsilon \frac{\beta_{max}}{k^2} e^Z Z^4 \left(\frac{u_*}{c} \max\left(cos(\theta - \emptyset), 0\right)\right)^2 \qquad (7)$$

Where ω is the angular frequency, ε is the air-water density ratio, k=0.4 (the von Karman constant) and β_{max} is a constant. C is the phase speed of the waves $\emptyset$ and $\theta$is the wave direction. Z is a wave age parameter.

The wave dissipation part of the source term is as follows:

$$S_{dis} = -C_{ds\,\langle\omega\rangle}(\langle k\rangle^2 m_0)^2 \left[(1-\delta)\frac{k}{\langle k\rangle} + \delta\left(\frac{k}{\langle k\rangle}\right)^2\right] N \qquad (8)$$

Where $m_0$is the total wave variance per m^2, k is the wavenumber and $\langle\omega\rangle$ and $\langle k\rangle$ are the mean angular frequency and mean wavenumber respectively. It is a steepness based closure parameterisation based on Komen et al. (1984).

This source term is generally successful in the prediction of Hs and Tp, however this parameterisation is known to have some problems in the accuracy in the growth of the wind-sea in the presence of swell. There can also be the problem of decreasing dissipation of swell with increasing swell steepness, which is contrary to observations (Ardhuin et al., 2009, Ardhuin et al., 2010).

2.3.4.2 Ardhuin et al. 2010 source terms (ST4)

The ST4 parameterization uses the wind input that is taken from WAM 4. It also has a sheltering term that creates an adhoc reduction of U_* in the higher frequencies. This allows a balance with the saturation-based dissipation that is used in this source term. This correction also reduces the drag coefficient at high winds. A sheltering coefficient $|S_u|$ ~1 is used to tune the wind stress in high winds which would be over-estimated where $|S_u| = 0$ (see equation 9 and 4.18 manual for full details, Tolman et al., 2014).

$$(u'_*)^2 = u_*^2\,(cos\theta_u,\, sin\theta_u\,) - |s_u| \int_0^k \int_0^{2\pi} \frac{s_{in}(k',\theta)}{C} (cos\theta, sin\theta)\, dk' d\theta \qquad (9)$$

The S_{in} term is an important part of the calculation of the wave supported stress; this is the output from the wave model that is then used in the calculation of a variable Charnock parameter (see equations 3 and 4). This calculation is very sensitive to the high frequency part of the wave spectrum. The sheltering term has the effect of reducing the S_{in} term in the ST4 source term compared to the ST3 wind input; this is shown in further detail in the following results section.

Observations of swell dissipation by Ardhuin et al. (2009b) are consistent with the effects of friction at the air-sea interface, this causes a flux of momentum from the waves to the wind. Swell dissipation is therefore included as a negative contribution and added to S_{in} to make the wind-wave source term.

The dissipation term follows Ardhuin et al. (2010) and is defined as a sum of a saturation-based term (Ardhuin et al., 2008a) and a cumulative wave breaking term. The cumulative breaking term is added to represent the smoothing of the surface by large breakers that wipe out waves of lower phase speed (see equation 10). This is based on observations of pre and post breaking wave spectra by Young and Babanin (2006), which showed that breaking waves suppressed shorter waves on the surface. Unlike the ST3 wave dissipation source the ST4 is based on a quantitative relationship with observed features of wave dissipation (Ardhuin et al., 2010).

$$S_{bk,cu}(k,\theta) = -1.44 C_{cu}\, F(k,\theta) \int_0^{r_{cu}{}^f} \int_0^{2\pi} max\left(\sqrt{B(k',\theta')} - \sqrt{B_r, 0}\right)^2 \Delta_C d\theta'\, dk' \quad (10)$$

Where r_{cu} defines the maximum ratio of the frequencies of long wave that will wipe out the short waves, taken as $r_{cu} = 0.5$ in Ardhuin et al. (2010). C_{cu} is a tuning coefficient that would be expected to be negative in the order of 1. B is the direction–integrated spectral saturation with a realistic threshold of $B_{0r} = 1.2 \times 10^{-3}$ corresponding to the onset of wave

breaking (Babanin and Young 2005, Ardhuin et al., 2010). B_r = 0.0009 was given as the threshold for the onset wave breaking in Ardhuin et al. (2010) that is consistent with the observations of Banner et al. (2000). $\Delta_c = |C - C'|$, which is the norm of the vector difference between the celerity of big breakers C' that wipe out smaller waves of phase speed C.

3. Results

3.1 The Wave Growth and Dissipation Terms in a Single Point Model.

In order to understand the different effects of the wave model source term physics on the Charnock parameter, it is useful to first look at the differences in the growth of the wave spectrum with each of the terms. In particular any differences in the S_{in} source term and the high frequency part of the spectrum will affect the calculation of the wave-induced stress. This is then used to calculate the Charnock parameter, which is passed to the atmosphere model.

A number of experiments were carried out using a single point model; the results are show in figures 5.1 to 5.5. The single point model was used to run the ST3 source term (E12D, Bidlot et al., 2012) and the ST4 term, given here as A451f (Ardhuin et al.,2010). A single constant wind speed was used for each of the tests shown. Outputs from each of the deep-water source terms and the total spectrum were taken at 3 hourly intervals (not all shown).

A number of differences between the ST3 (E12D) source term and ST4 (A451f) are apparent. In particular there are significant differences in the growing wave spectra between A451f and E12D. It is immediately obvious that the spectrum for the A451f contains less total energy after 6 hours than the spectra calculated from the ST3 source term physics (figure 3.1). Two other points are noted; the S_{in} term for A451f is smaller (figure 3.1) and the dissipation term is quite different with nearly all the wave energy being dissipated at the spectral peak (figure 3.1). This then leads to a different response from the non-linear source term (S_{nl}); considerably less energy is transferred from higher to low frequencies (figure 3.1). This appears to be in part due to greater dissipation of longer period wave energy at the peak of the spectrum by $S_{dis.}$ At 18 hours into the run the difference in the S_{in} and S_{dis} sources terms in A451f is still evident. As the spectrum develops the non-linear source term for A451f is now transferring more energy to the lower frequencies, resulting in a lower peak frequency (figure 3.2). After 30 hours run time, the energy density spectrum for the A451f is closer to the ST3 spectrum (figure 3.3). There is still a lower wind energy input over the whole of the resolved energy spectrum for A451f and even after 30 hours there is still a significant difference in Hs between ST3 and ST4. The S_{dis} has now reduced at the peak of the spectrum for A451f and this is allowing more energy to be redistributed to the lower frequencies by S_{nl}. The S_{nl} term is now similar for the ST3 and ST4 terms.

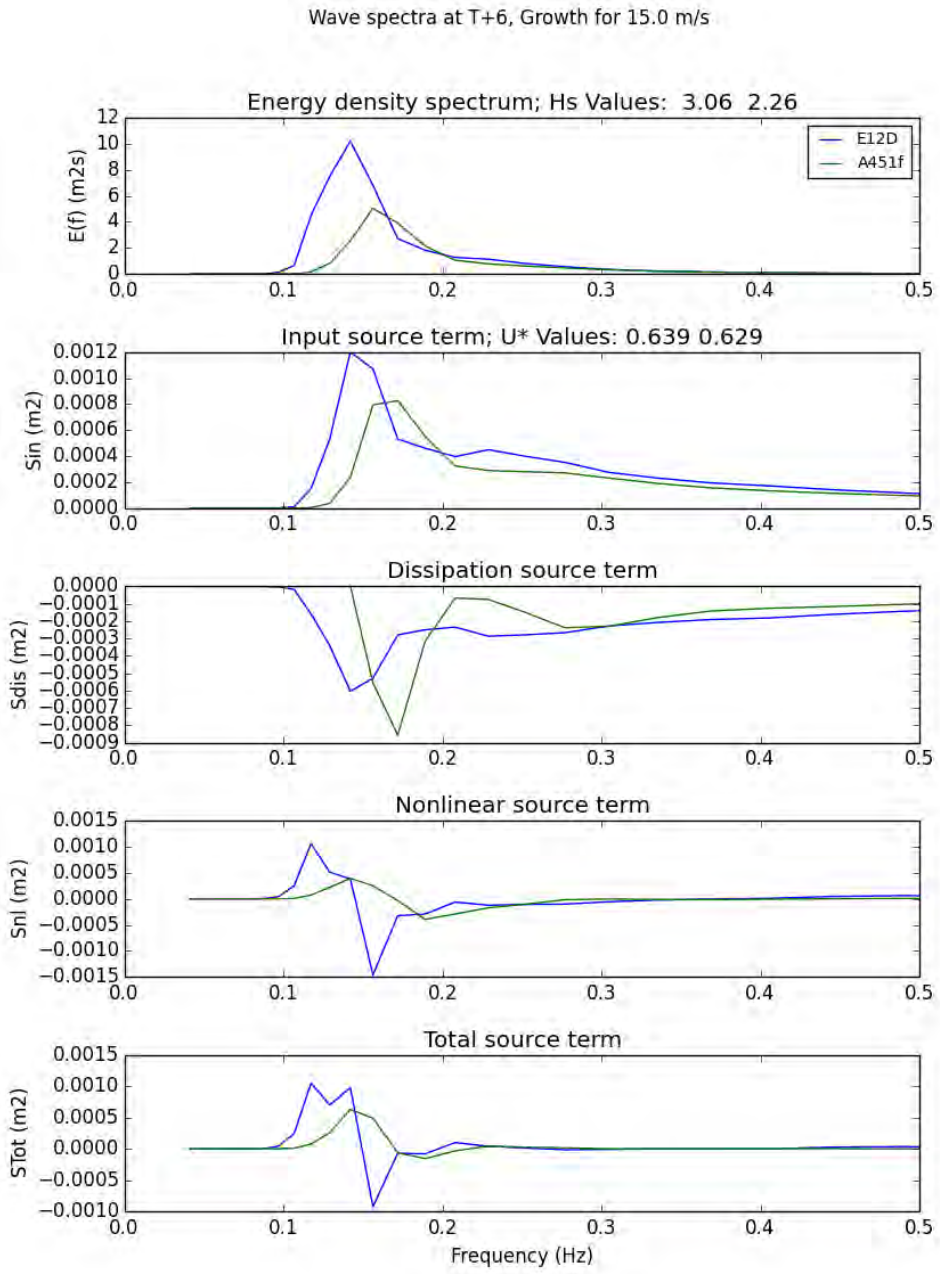

Figure 3.1 Wave spectra growth after 6 hours at 15 ms-1 from top to bottom: total energy density, $S_{in.}$ S_{dis}, S_{nl} and total of all source terms.

A wind speed of 5ms^{-1} has been chosen to illustrate the difference between the two source terms in low winds. A similar result is seen as for the higher wind speed cases. After 6 hours the E12D (ST3) wave spectrum contains more energy than A451f (see figure 3.4). This demonstrates that even at low wind speeds the ST3 source term results in a faster growing wave spectrum than ST4. The Sin term is again larger for the ST3

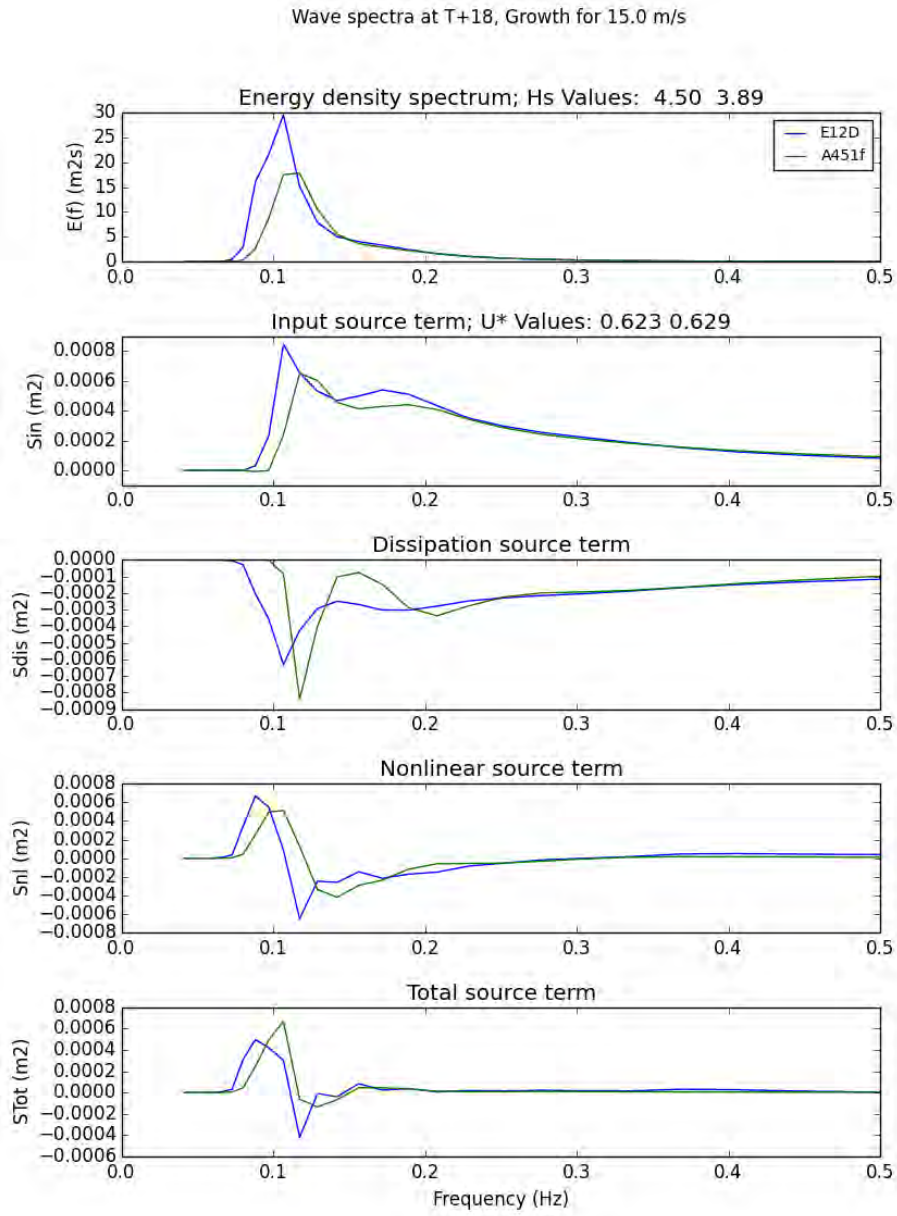

Figure 3.2 Wave spectra growth after 18 hours at 15 ms-1 from top to bottom: total energy density, $S_{in.}$ S_{dis}, S_{nl} and total of all source terms.

source term. As the wave spectrum develops the dissipation starts to decrease at the spectral peak for the ST4 source term. This causes the ST4 spectrum to begin to 'catch up' with the ST3 wave spectrum. After 30 hours (figure 3.5) the energy in the wave spectra for both source terms is now similar. The S_{in} term remains larger for the ST3 source term; however this is balanced by the larger S_{dis}. In the case of the ST4 term the dissipation of wave energy at the spectral peak is now reduced.

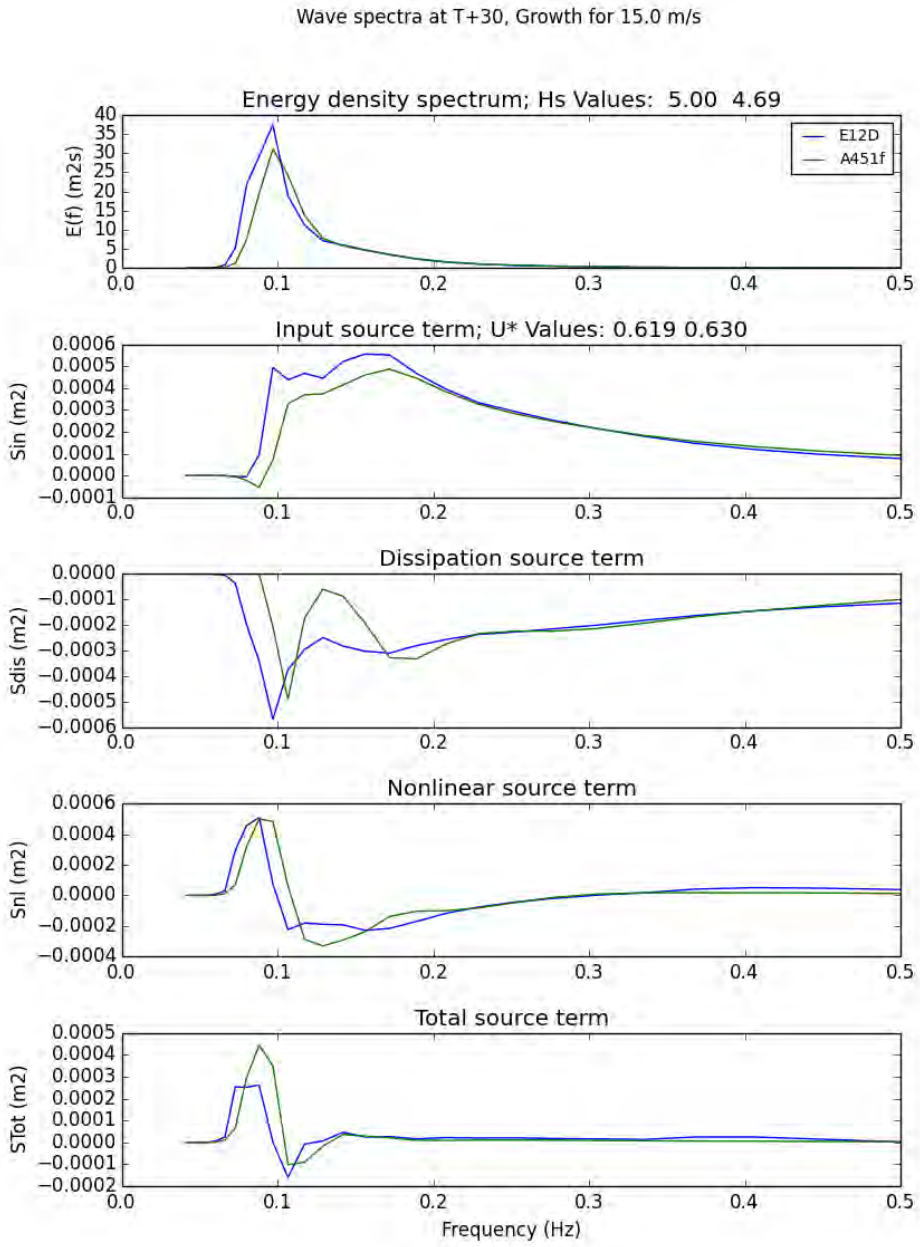

Figure 3.3 Wave spectra growth after 30 hours at 15 ms-1 from top to bottom: total energy density, S_{in}, S_{dis}, S_{nl} and total of all source terms

In summary the wave spectrum develops more slowly towards a more 'fully developed' shape with ST4 than with ST3. The ST4 Sin term includes a sheltering term for the high frequency wave energy; this reduces the input of wind energy at these frequencies and further slows spectral growth. This will also result in a different wave induced stress for the ST3 and ST4, with the latter being smaller. It is noted above however that the U^*

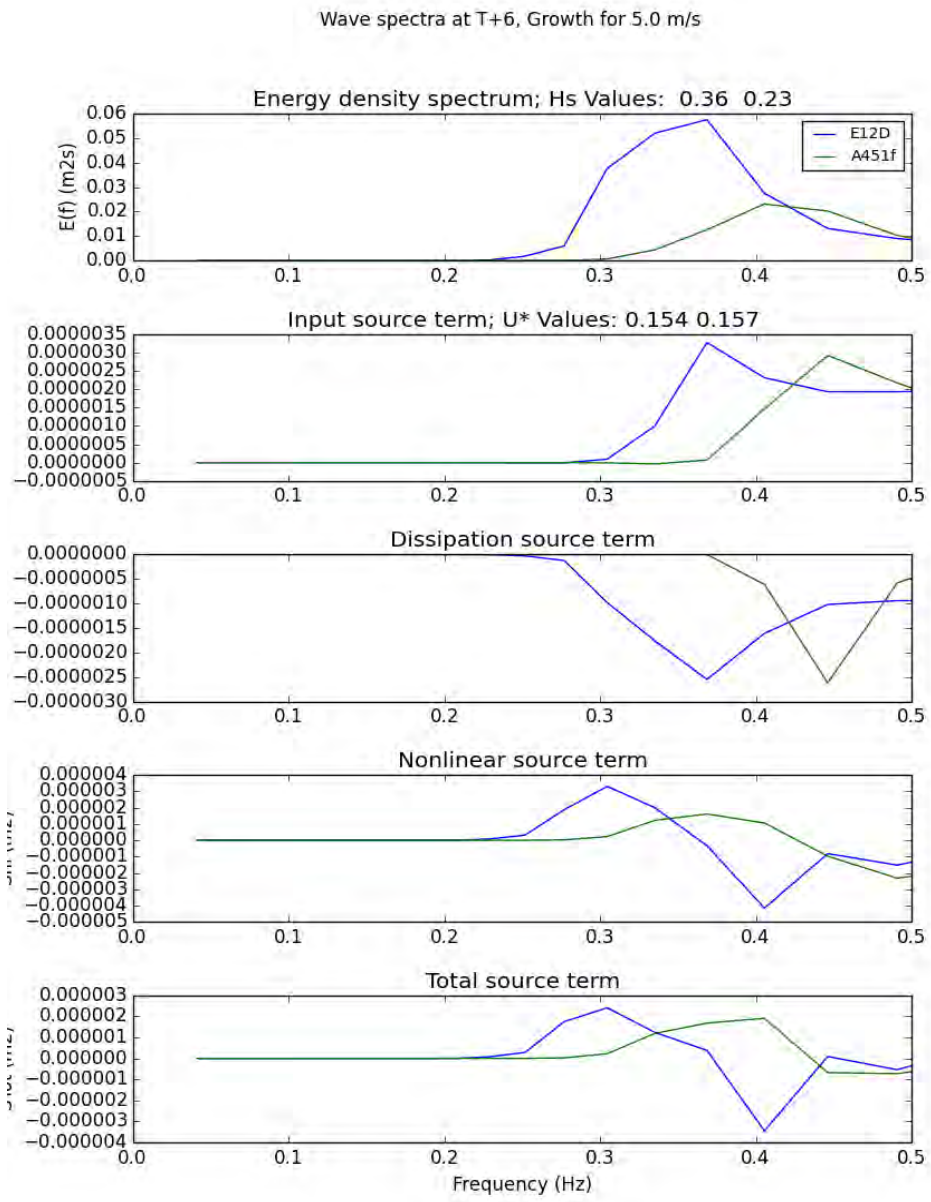

Figure 3.4 Wave spectra growth after 6 hours at 5 ms-1 from top to bottom: total energy density, S_{in}, S_{dis}, S_{nl} and total of all source terms

values are similar for both source terms. The ratio of the wave-induced stress to the air-side stress will affect the value of the Charnock parameter calculated using the two different source terms. In the case of the ST4 source term the smaller values of S_{in} will result in a smaller wave-induced stress term than for ST3 in the same wind conditions. This has the effect of increasing the value on the bottom half of equation 3, which in turn results in a smaller value for the Charnock parameter from the ST4 source term in principle; see equations 3 and 4 in section 1.3.2. However the ST4 source term used in

our experiments has a larger $\hat{\alpha}$ value of 0.01 (compared to 0.006 for ST3). Therefore despite the smaller S_{in} values with ST4 this source term produces larger Charnock values.

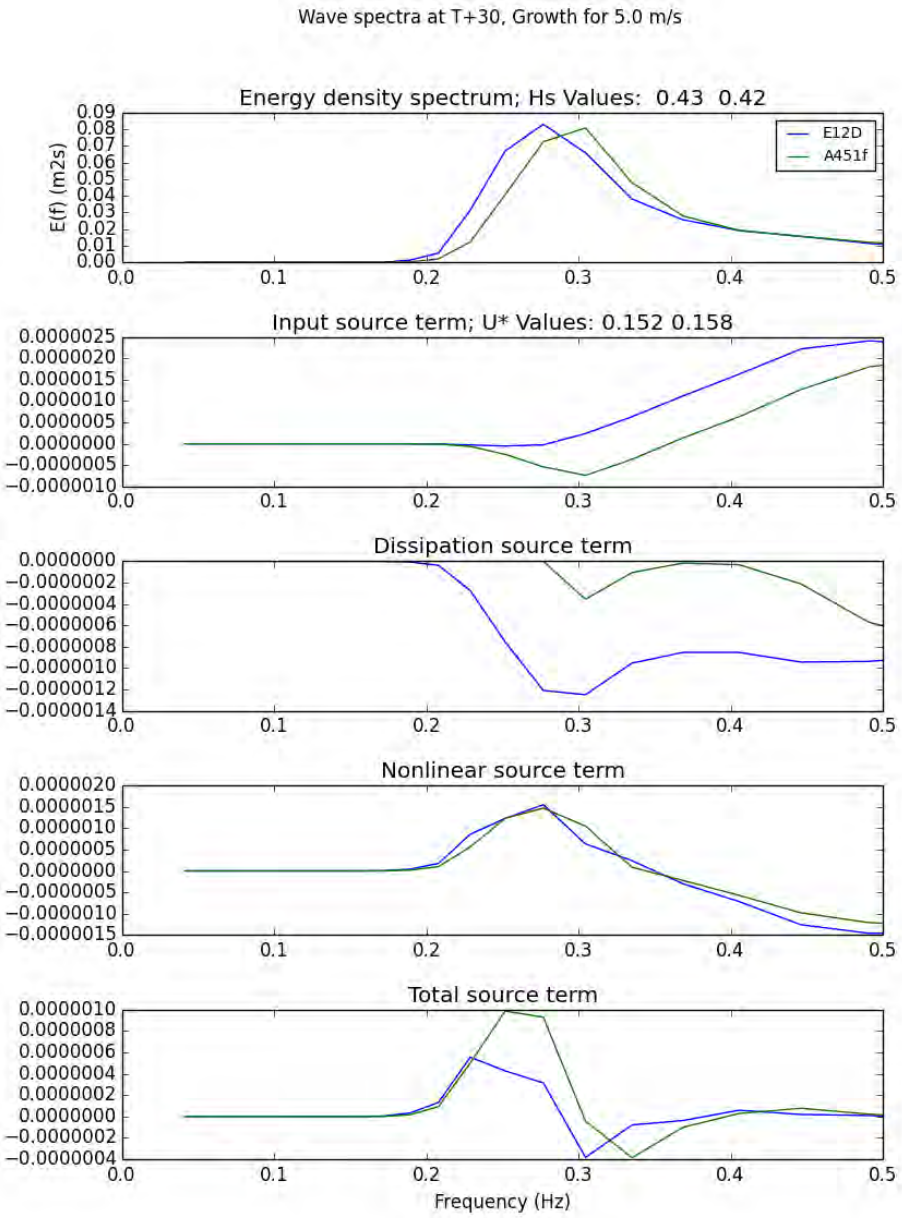

Figure 3.5 Wave spectra growth after 30 hours at 5 ms-1 from top to bottom: total energy density, S_{in}. S_{dis}, S_{nl} and total of all source terms

3.2 Sensitivity of the atmosphere-wave coupled model to source term physics.

3.2.1 Patterns in Charnock parameter

Overall, the variable Charnock parameter calculated by the wave model is less than the constant 0.018 value used by the atmosphere only model. This is the case for both the ST4 physics (shown in figure 3.6) and the ST3 (figure 3.7). Although the average value of the Charnock parameter is different for each of the source terms the overall geographic and seasonal patterns are very similar. The largest values for the Charnock parameter are seen in the storm belt regions, where rougher sea-states occur. The lowest values occur near the equator. In these regions the Charnock value is close to 0.006 for the AW-ST3 run, which is the default minimum Charnock value when the wave-induced stress is close to zero.

In principle, ST4 Charnock parameter values might be expected to be smaller than those from ST3. However, in the physics settings implemented the ST4 run used a minimum Charnock value of 0.01 versus 0.006 for ST3, so the resulting mean Charnock parameter is larger for ST4. This is consistent with a distribution of wind speeds that is aliased toward more frequent, less windy conditions. Although the mean values of the Charnock parameter calculated in AW-ST4 are larger, the variability of the parameter, especially in the major storm belt regions is greater in AW-ST3 (figures 3.8 – 3.11), indicating the slightly higher sensitivity to S_{in} noted in section 3.1.In DJF (see figure 3.8) AW-ST3 has a larger variability in the area associated with high storm track density in the North Atlantic. The distribution of the Charnock parameter in AW-ST4 is relatively flat in comparison (figure 3.9).

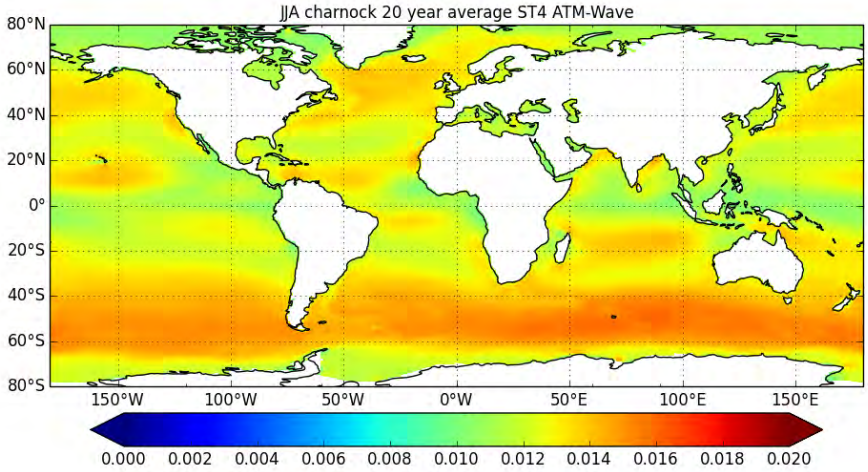

a)

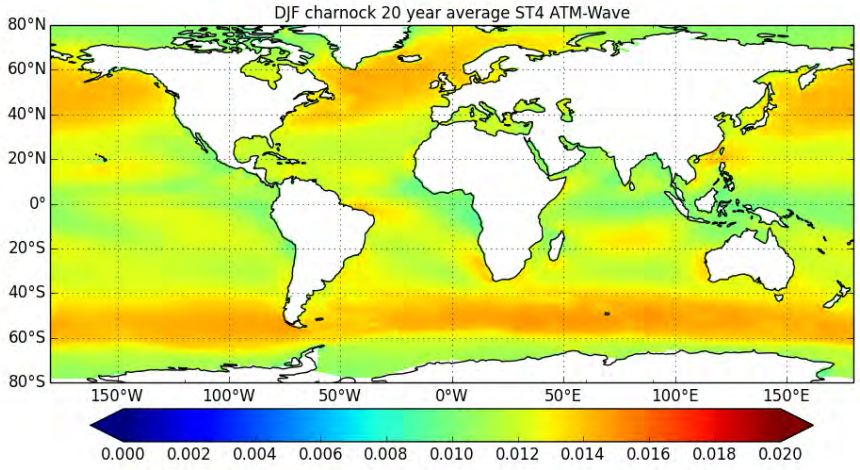

b)

Figure 3.6 The average a) JJA and b) DJF seasonal Charnock values for ST4 source terms (AW-ST4)

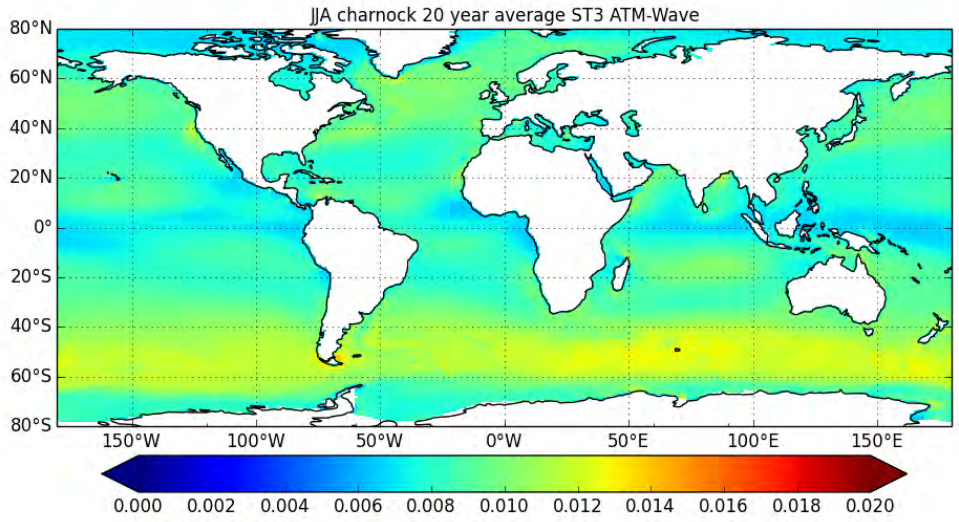

a)

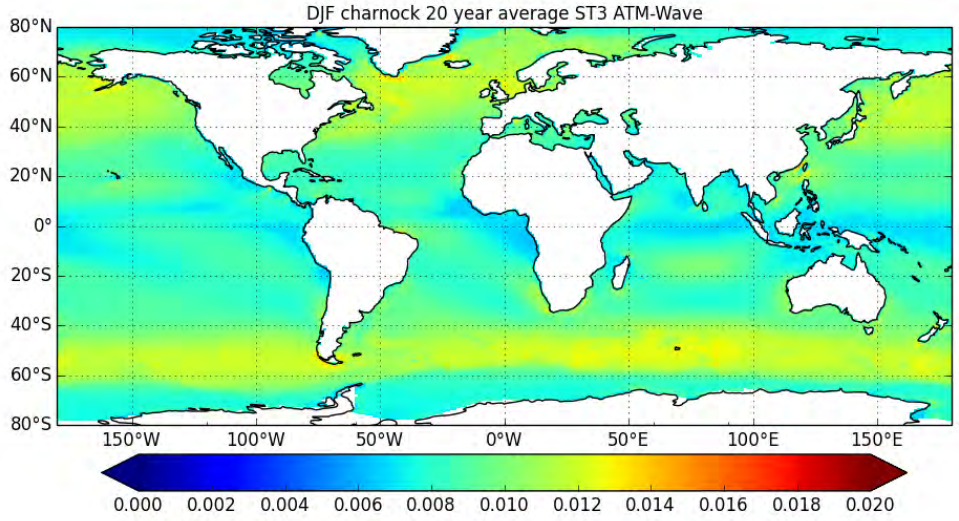

b)

Figure 3.7 The average a) JJA and b) DJF seasonal Charnock values for ST3 source terms (AW-ST3)

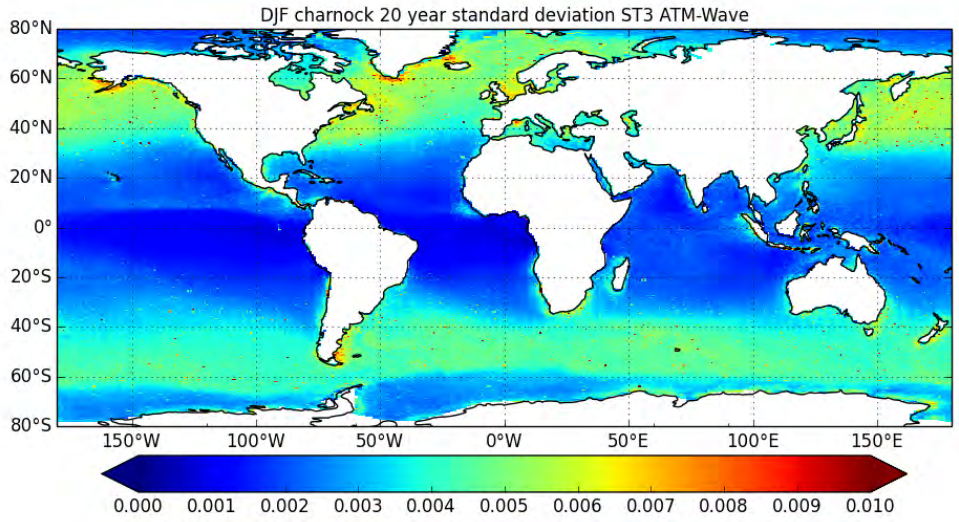

Figure 3.8 DJF Standard deviation of the Charnock parameter for AW-ST3

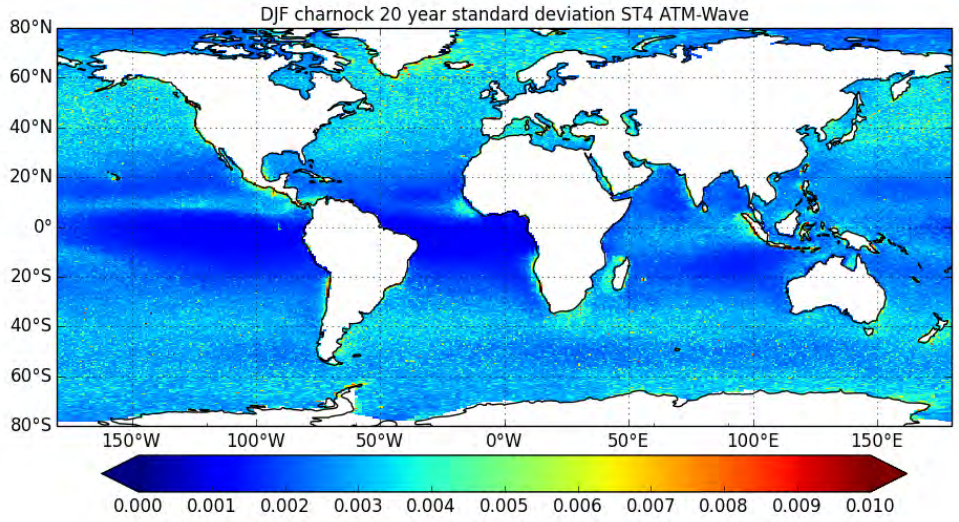

Figure 3.9 DJF Standard deviation of the Charnock parameter for AW-ST4

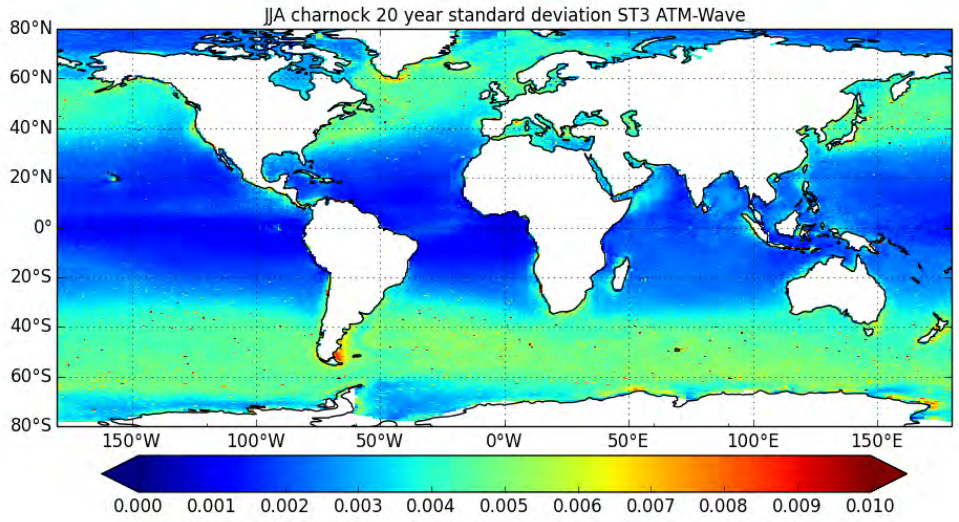

Figure 3.10 JJA Standard deviation of the Charnock parameter for AW-ST3

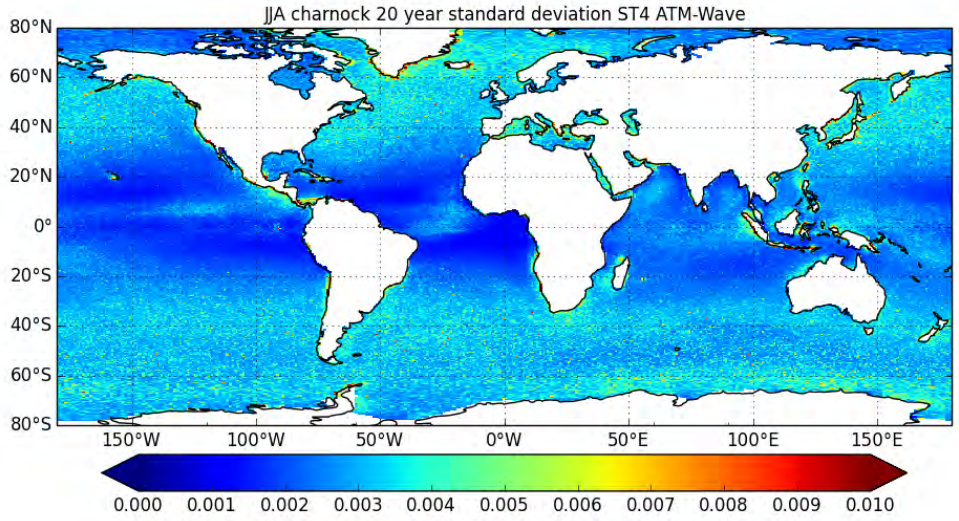

Figure 3.11 JJA Standard deviation of the Charnock parameter for AW-ST4

3.2.2 Changes in the Scalar 10m wind speed.

Figure 3.12a shows the difference between the coupled run with ST4 physics (AW-ST4) and the control run (ATM) for the scalar wind speed in DJF, the same difference plot for the coupled run using ST3 wave model physics (AW-ST3) and the control run (ATM) is shown in 3.12b. In general in many parts of the globe there is an increase in the 10m wind speed, especially in the southern hemisphere. In the JJA season increases in the wind speed occur in the northern hemisphere and parts of the southern hemisphere (figure 3.13).

Changes in the scalar wind speed for AW-ST4, using the ST4 physics package show greater variability than AW-ST3. The nature of the changes appear to be fetch related, with decreased wind speeds in regions of relatively short fetch. The most sensitive area to the variable Charnock parameter is the east North Atlantic. In particular the wind speed is reduced around the storm belt region. Changes to the wind stress largely reflected the changes to the scalar wind speeds, details are given in the appendices.

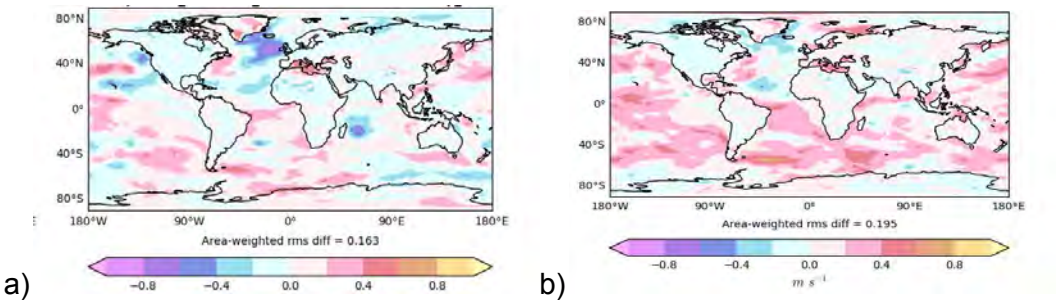

Figure 3.12 Difference between control ATM run and UM-WAVEWATCH coupling (Experiment – Control) for the a) ST4 (AW-ST4) and b) ST3 (AW-ST3) in DJF.

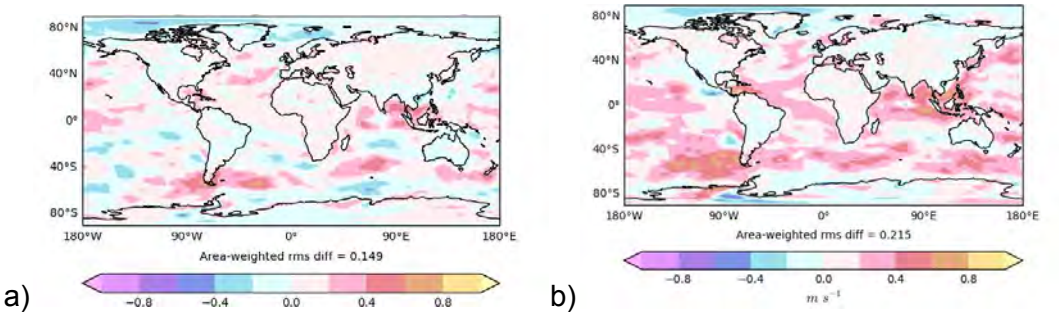

Figure 3.13 Difference between control ATM run and UM-WAVEWATCH coupling (Experiment – Control) for the a) ST4 (AW-ST4) and b) ST3 (AW-ST3) in JJA

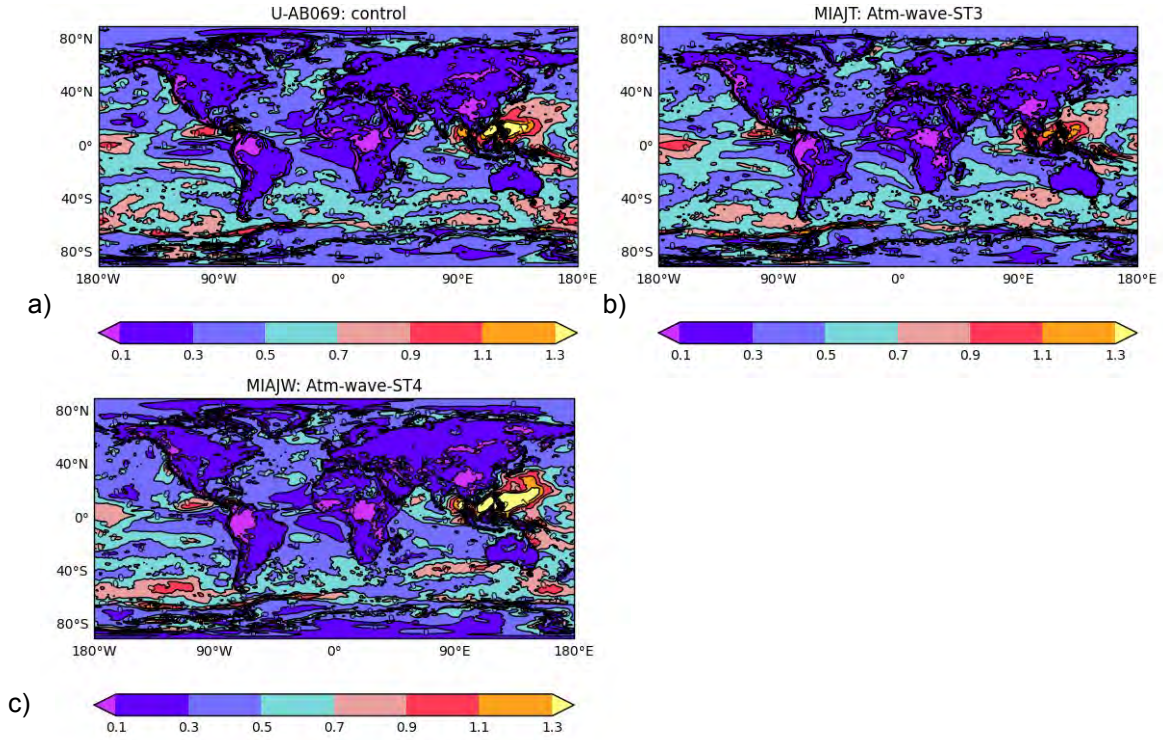

Figure 3.14 The standard deviation (of annual means) for the scalar wind speed for a) ATM (control) b) AW-ST3 (Atm-wave-ST3) and c) AW-ST4 (Atm-wave-ST4) in JJA.

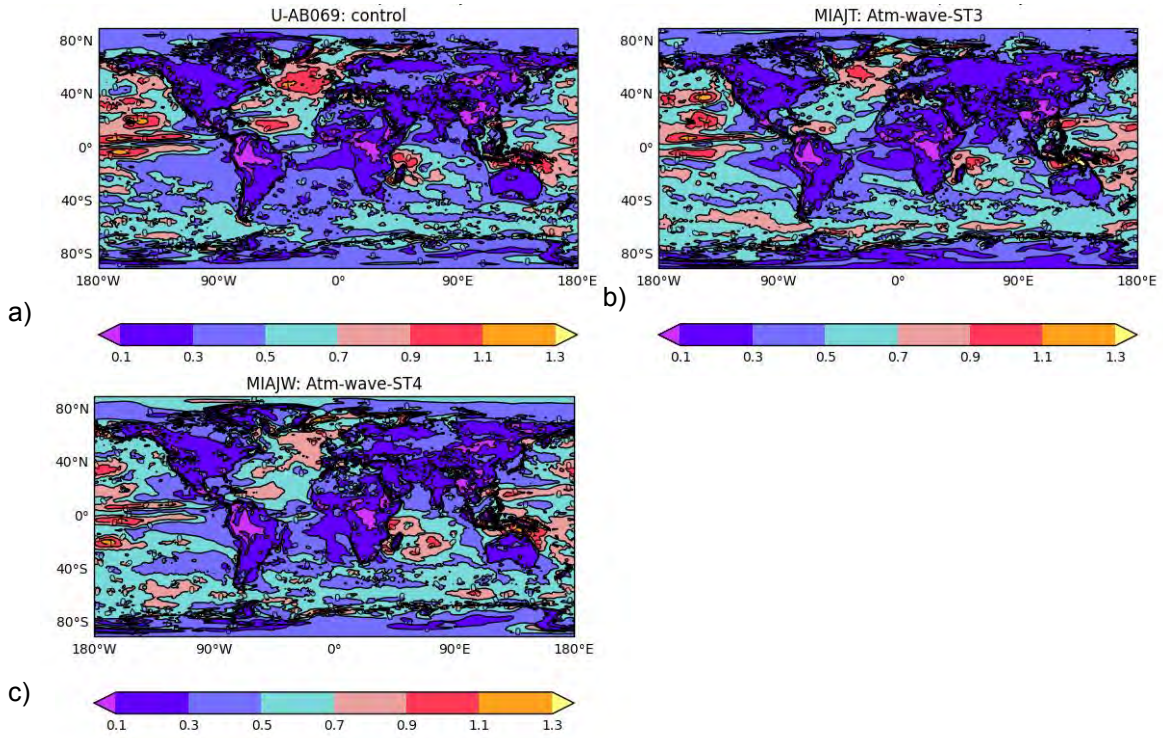

Figure 3.15 The standard deviation (of annual means) for the scalar wind speed for a) ATM (control) b) AW-ST3 (Atm-wave-ST3) and c) AW-ST4 (Atm-wave-ST4) in DJF.

Overall larger Charnock values occurred in AW-ST4, however the average seasonal values were still less than the UM model default of 0.018. Therefore in most ocean locations of the globe an increase in wind speed occurred in the AW-ST4 experiment (Figures 3.12 and 3.13). This increase is due to less momentum being taken from the atmosphere by the waves than in the control (ATM). In the case of AW-ST3 the seasonal average of the Charnock was reduced even further, therefore the wind speeds were increased almost everywhere (compared to ATM) to a greater extent than in AW-ST4. The exception to this in the case of both experiments is the North Atlantic where wind speeds are reduced in the storm track regions during DJF.

The significance of the changes to the scalar wind speed were assessed initially by comparing the standard deviation of the 3 runs, these are shown in figures 3.14 and 3.15 above. In JJA (figure 3.14) the variability of the wind speed is not very different between the 3 runs; there is some reduction in the eastern equatorial pacific for AW-ST3 but the pattern of variability is largely the same. The increase in the wind speed seen in the Southern Ocean for JJA (figure 3.14b) is similar to the standard deviation of the control, in most cases it is not greater, which suggests that the changes in wind speed due to the wave coupling are not larger than the general variability of the wind speeds.

In DJF (figure 3.15) however there are some changes to the variability in both hemispheres. In the North Atlantic the variability of the scalar winds has been reduced in both AW-ST3 and AW-ST4, the largest reduction is seen in AW-ST4. The reduction in wind speed in the NA for AW-ST4 minus ATM is not larger than the standard deviation of the wind speed in this region in the ATM run. The reduction of the variability in the wind speeds for this region suggests that in some cases during storm events the variable Charnock parameter may have led to a reduction of the highest wind speeds. This will require further investigation however. In the case of both source terms there has been an increase in the standard deviation in the Southern Ocean during JJA.

A direct comparison between the AW-ST3 and AW-ST4 runs shows globally faster wind speeds with AW-ST3 (figures 3.16 and 3.17). Here the errors of the two runs are also shown, compared to a climatological data set. The pattern of wind speed bias is very similar between the two experiments; however the positive biases are generally greater for the AW-ST3 than for AW-ST4, particularly in the Southern Ocean winter (figure 3.17 c and d).

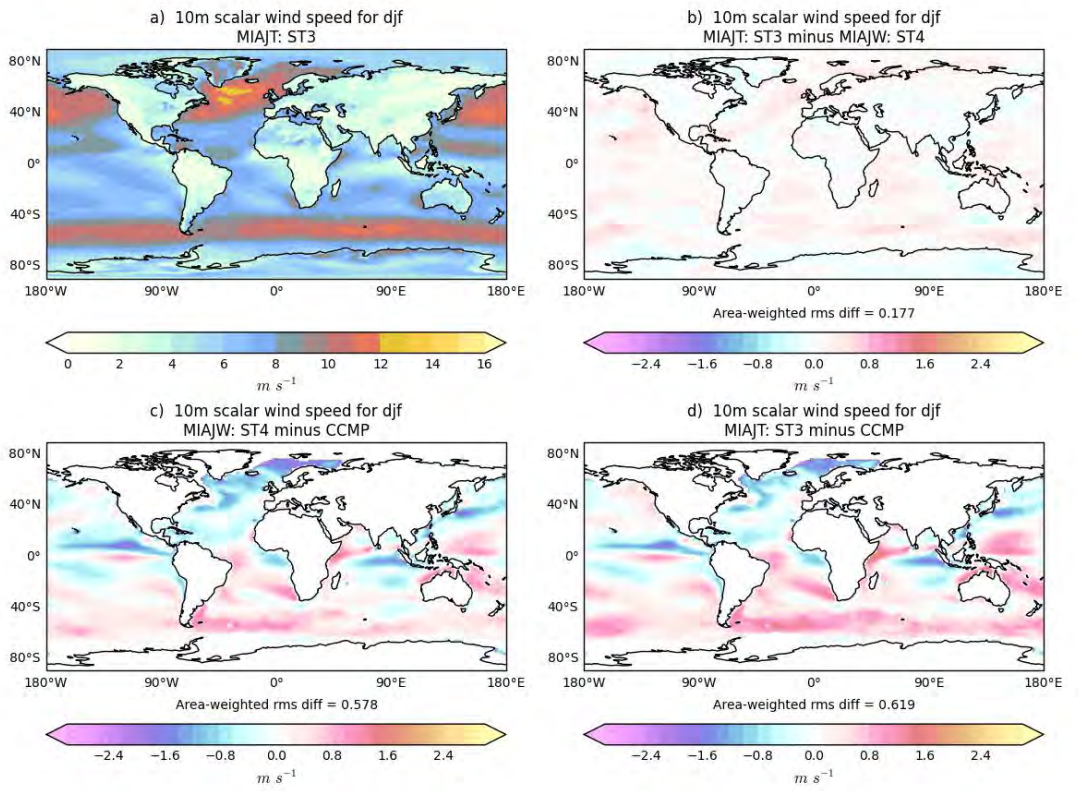

Figure 3.16 The 10m scalar wind speeds for AW-ST3 in the DJF season: a) scalar wind speed, b) difference AW-ST3-AW-ST4 c) bias AW-ST4 d) bias AW-ST3 compared to Cross-Calibrated Multi-Platform wind vector analysis product (CCMP).

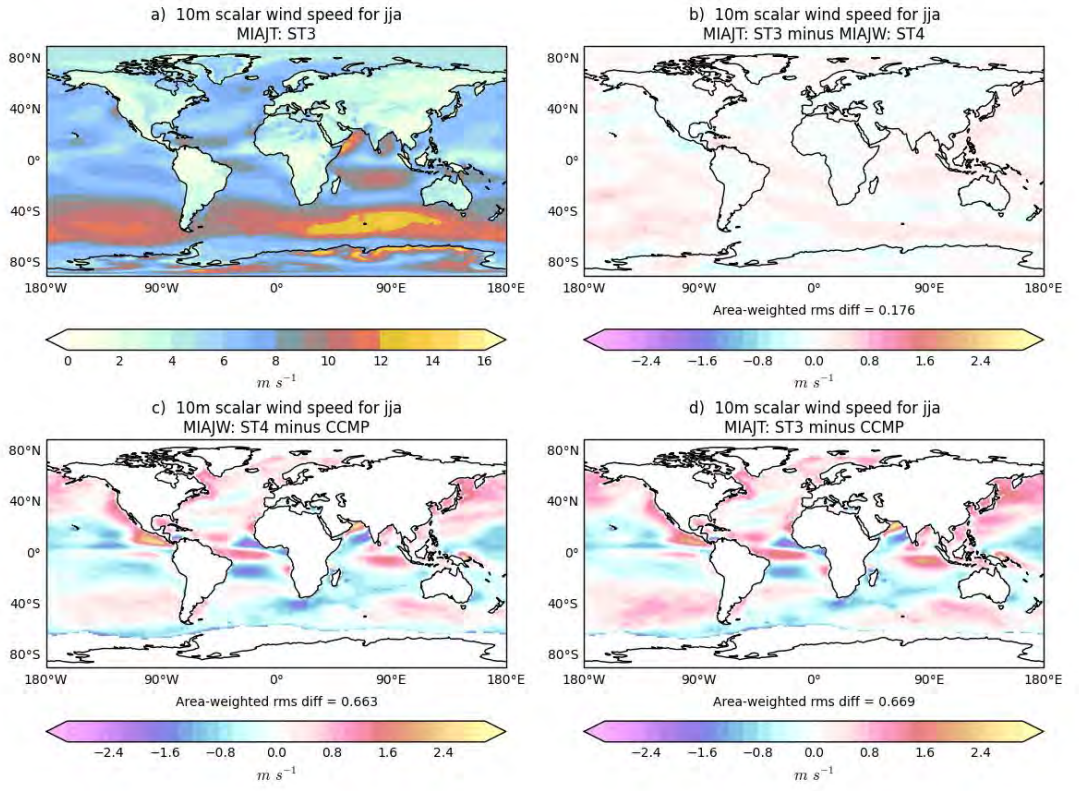

Figure 3.17 The 10m scalar wind speeds for AW-ST3 in the JJA season: a) scalar wind speed, b) difference AW-ST3-AW-ST4 c) bias AW-ST4 d) bias AW-ST3 compared to Cross-Calibrated Multi-Platform wind vector analysis product (CCMP).

3.3 Wave Coupling Impacts on Storm Tracks.

A storm track analysis was carried out on the atmosphere model outputs for the North Atlantic during DJF. The approach used was that of Hoskins and Hodges (2001), using a range of fields including the Pressure at Mean Sea Level (PMSL), 500ha geopotential height and lower tropospheric vorticity. The Eulerian diagnostics are computed using a bandpass filtered variance statistic. The feature tracking of systems was computed by minimizing a cost function for the ensemble track smoothness to obtain the minimal set of the smoothest tracks. An intensity threshold of (in the filtered field) above which a feature is identified to be present is required for the feature tracking along with the maximum displacement distance and the smoothness required for the track. Track densities are then computed as a probability density function. The genesis density, the density of where systems originate is computed from the starting point of the tracks.

The results are shown in figures 3.18, 3.19 and 3.20. There is an increase in the genesis density in the northwest Atlantic near the coast of the USA in AW-ST4 compared to ATM. The increase is not large and may well be within the expected variability, however it also corresponds to an increase in the wind speed in the AW-ST4 experiment in the same area (figure 3.19 g) and f)). The genesis intensity over the NE Atlantic has been reduced in AW-ST4, there is also a decrease in the mean intensity in this area (see figure 3.18 and 3.19 g) and f)).

The changes in the storm track intensity are not as large in the AW-ST3 experiment compared to the ATM control (figures 3.20 h) and f)). There is a reduction in the genesis density in the NE Atlantic however (figure 3.19 h) and f)). The reduction in storm track intensity appears to be related to the reduction in the wind speeds during DJF in AW-ST4 and AW-ST3, particularly in the NE Atlantic. There is some increase in the winds in parts of the West Atlantic, which occur in the same regions on increased wind speeds in DJF (figure 3.12).

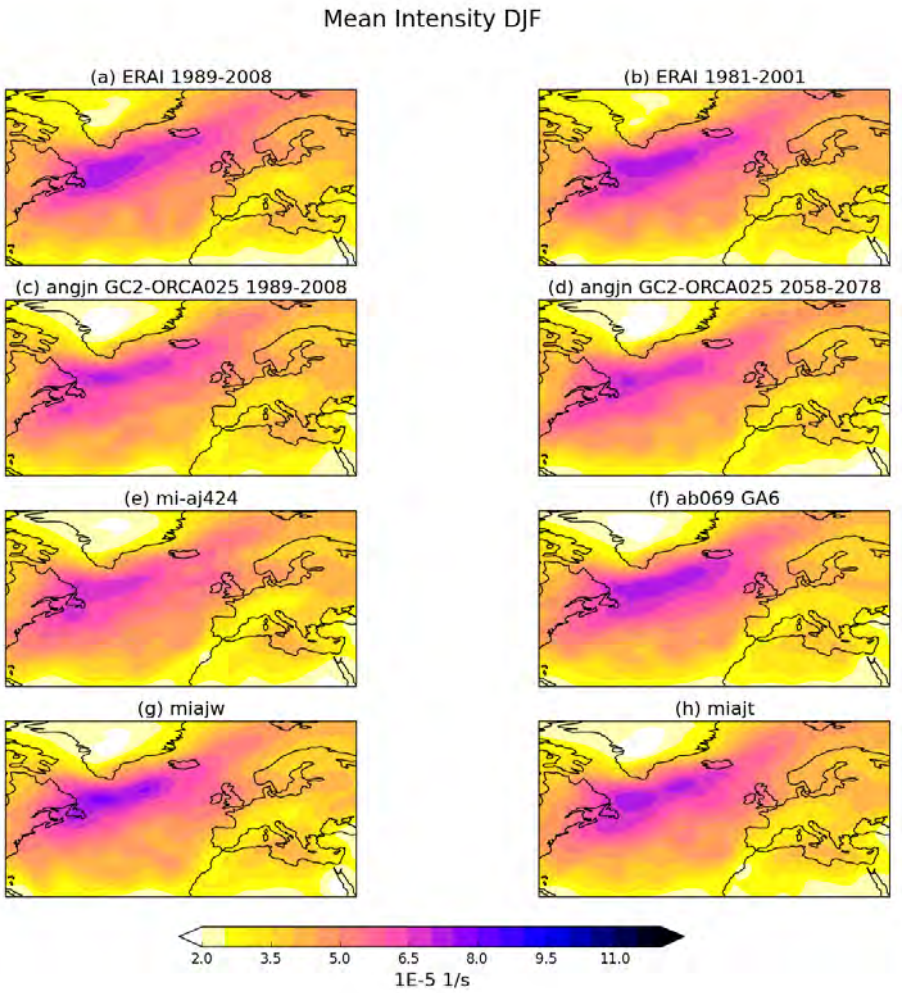

Figure 3.18 Mean intensity of storm tracks in DLF in the Gulf Stream region for a) ERA1 (1989-2008), b) ERA1 (1981-2001), c) AO (GC2-ORCA025), d AO 2058-2078 (GC2-ORCA025), e) AOW, f) ATM, g) AW-ST4, h)AW-ST3

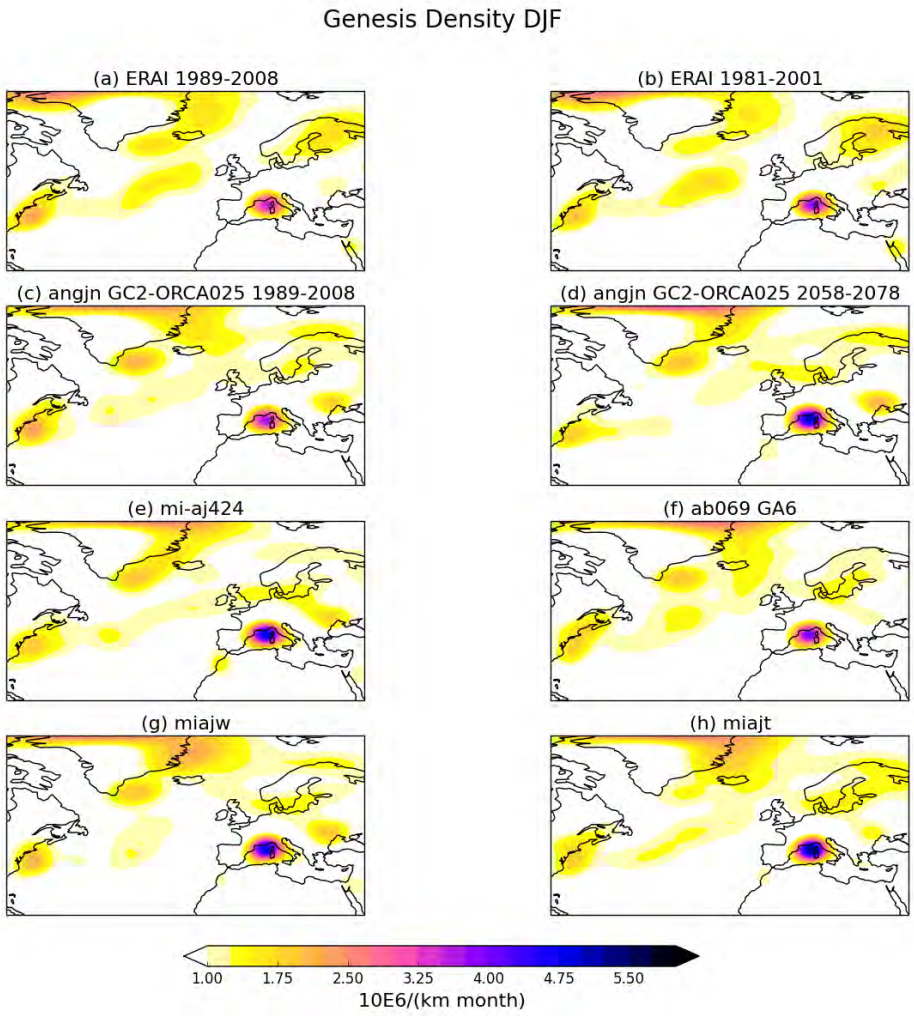

Figure 3.19 Genesis Density of storm tracks in the gulf stream region in DJF for a) ERA1 (1989-2008), b) ERA1 (1981-2001), c) AO (GC2-ORCA025), d AO 2058-2078 (GC2-ORCA025), e) AOW, f) ATM, g) AW-ST4, h)AW-ST3

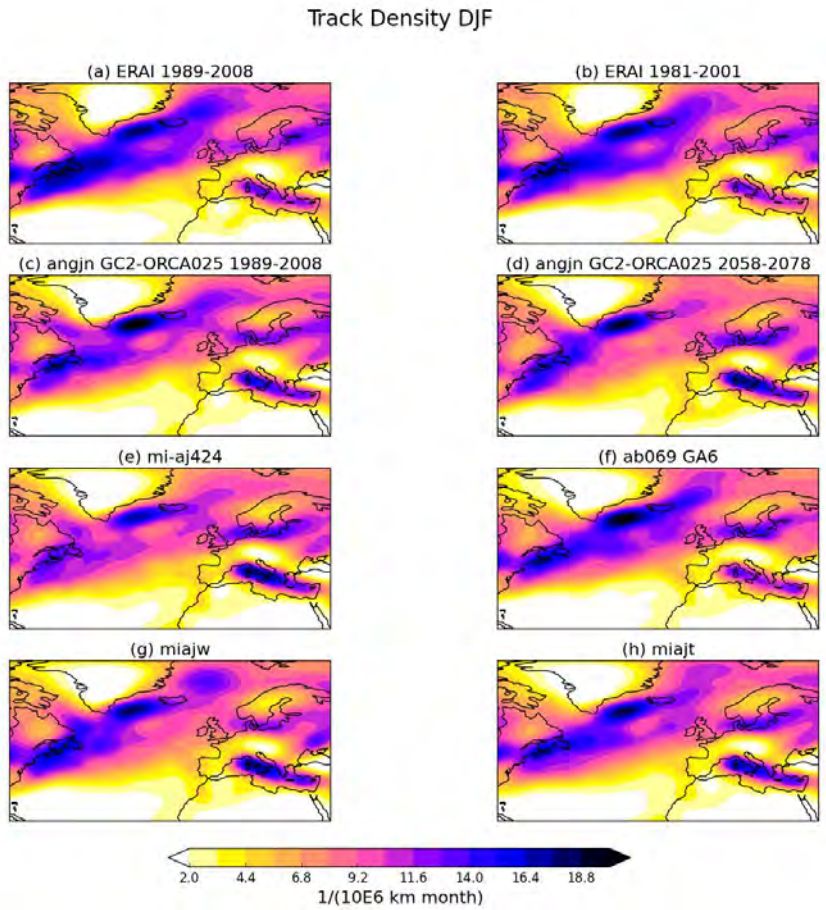

Figure 3.20 Storm track density during the DJF in the Gulf Stream region for each of the experiment and control runs a) ERA1 (1989-2008), b) ERA1 (1981-2001), c) AO (GC2-ORCA025), d AO 2058-2078 (GC2-ORCA025), e) AOW, f) ATM, g) AW-ST4, h)AW-ST3

3.4 Precipitation sensitivities to wave coupling

In the North Atlantic winter, changes in the precipitation patterns for DJF are shown in figure 3.21. There is an increase of about 1mm/day in the northwest of the North Atlantic around the Gulf Stream and parts of the Labrador Sea. In the north-eastern parts of the North Atlantic and north of the UK around 50°-65° N however, there is a decreased precipitation of approximately 1-2mm/d. The decrease precipitation also occurs where there is an increase in the 500mb height (see appendices).

The increase in precipitation in the North Atlantic, is likewise largely in an area where the greatest storm track densities occur and there are some increases in wind speed seen in areas near the east coast of the USA. However the increase in precipitation is also extended further east into the North Atlantic. With the exception of the North Atlantic, changes in the precipitation rates are largely in the low to mid-latitudes between the equator and 40° N/S. Precipitation is decreased by up to 3mm/d in parts of the equatorial Pacific between 180° and 90° W. There is also an increase in the precipitation around the equator of about 1mm/d. There are some significant differences in precipitation patterns North of Australia and over Indonesia and a reduction in precipitation in the Indian Ocean just east of the African continent.

In JJA changes in the precipitation are largely in the southern hemisphere and again between 0° and 40° S., these are shown in figure 3.22. The most significant changes in the pattern are seen to the north of Australia and in parts of the Indian Ocean. There is an increase in the precipitation north of Indonesia of about 1mm/day, while over this region there is a decrease of about 2mm/day. This could be due to changes to the storm track in the southern hemisphere winter. There is an increase in the surface wind speed that generally corresponds to the areas of increased precipitation (figure 3.12b and 3.13b).

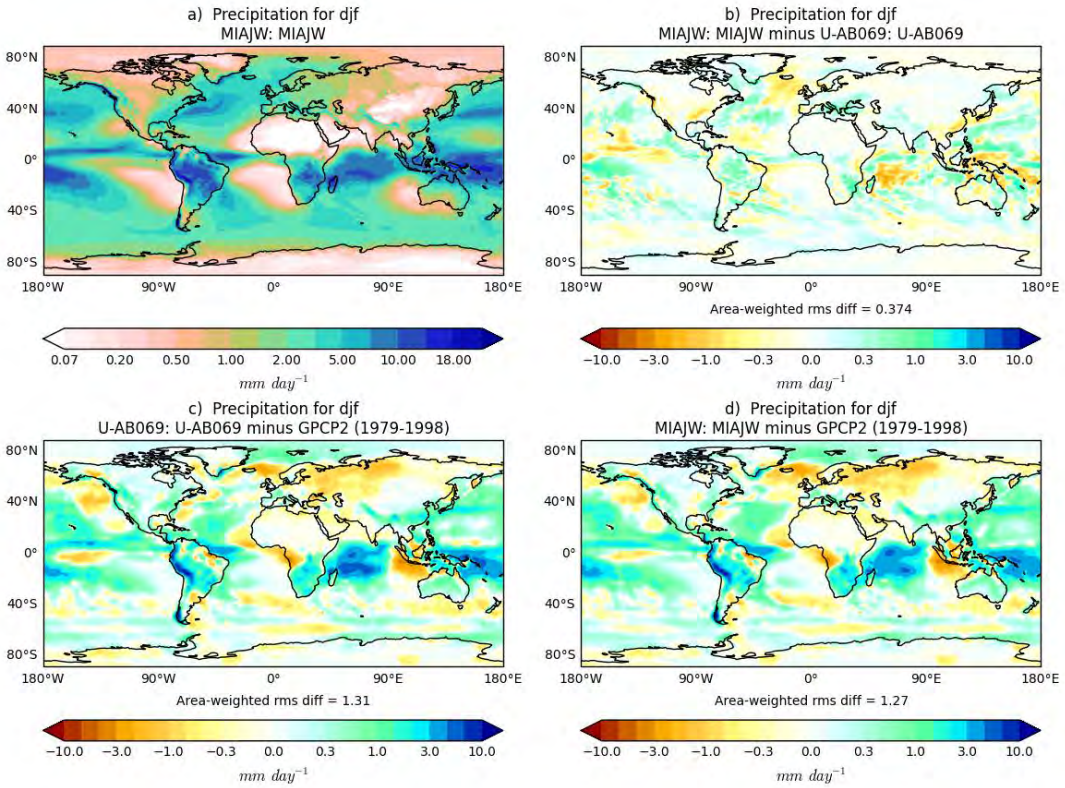

Figure 3.21 Precipitation changes for AW-ST4 – AO (control) in DJF: a) AW-ST4 seasonal precipitation, b) difference AW-ST4 (ST4) – AO, c) bias AO, d) bias AW-ST4

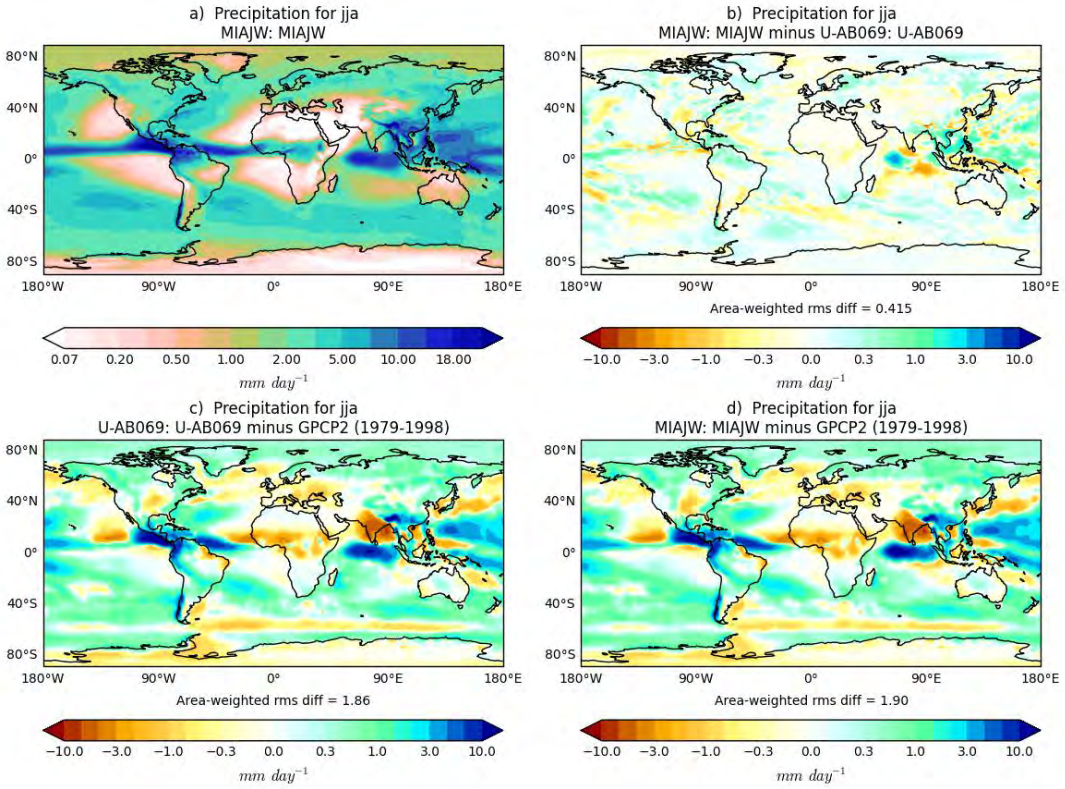

Figure 3.22 Precipitation changes for AW-ST4 – AO (control) in JJA: a) AW-ST4 seasonal precipitation, b) difference AW-ST4 (ST4) – AO, c) bias AO, d) bias AW-ST4

4. Ocean-Wave Atmosphere coupling sensitivities

4.1 Charnock Patterns

There are some differences in the seasonal Charnock averages between AW-ST4 and the AOW experiment (figure 4.1a and b). The overall pattern of Charnock values is similar but there are some differences in detail, particularly in the North Atlantic and Indian Ocean. There are higher DJF Charnock values in the northern hemisphere in AOW (figure 4.1b), these are probably due to the higher wind speeds described further in the following section.

There are also some changes in the storm track intensities around the Gulf Stream area, these were shown in section 3. The differences between the different experiments are small, however there is a reduction in the storm track intensity for AWO, see figure 3.20 c) and e). The mean intensity for the all the ocean coupled runs is also less than the ERA1 and the atmosphere only runs (figure 3.18).

4.2 Precipitation and 10m Scalar Winds

The mean seasonal differences in the scalar wind speed for AOW and the control (AO) are shown in figures 4.2 and 4.3. The pattern of changes in the wind speeds are different from those that were seen in the atmosphere-wave coupled run (AW-ST4). There is an increase in the wind speed in equatorial regions in both DJF and JJA. The Pacific Ocean has increases of about 0.4 m/s in most areas. Although there are still some areas where the wind speed is decreased, these are mostly coastal regions. The storm belt region of the Southern Ocean has some significant increases in wind speed in high latitude areas of up to 1m/s. There is still a decrease in the wind speeds in parts of the North Atlantic during the northern hemisphere winter. Around the mid-north Atlantic however there is now an increase in the wind speed during this season. This indicates that there is a feedback from the Gulf Stream that has changed the wind patterns in this region.

The variability of the wind speeds are shown in figures 4.4 and 4.5 as standard deviations. There is not a large change in the variability of the winds during the JJA season. There is however some increase in the standard deviation in the North Atlantic, with an increase shown for the AOW run. This increase in variability occurs in the same regions where an increase in the wind speed has occurred during the DJF season for the AOW run. This increase in variability did not occur in the AW-ST4 experiment.

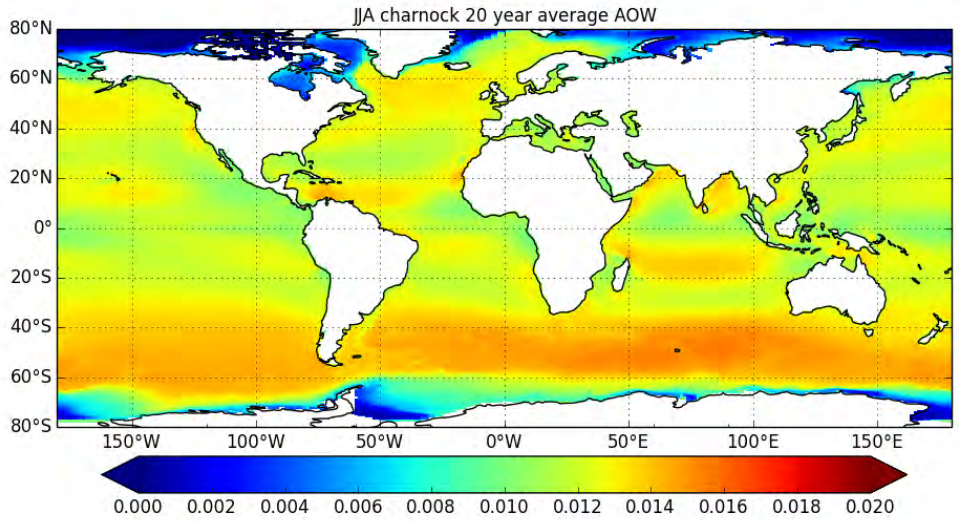

a)

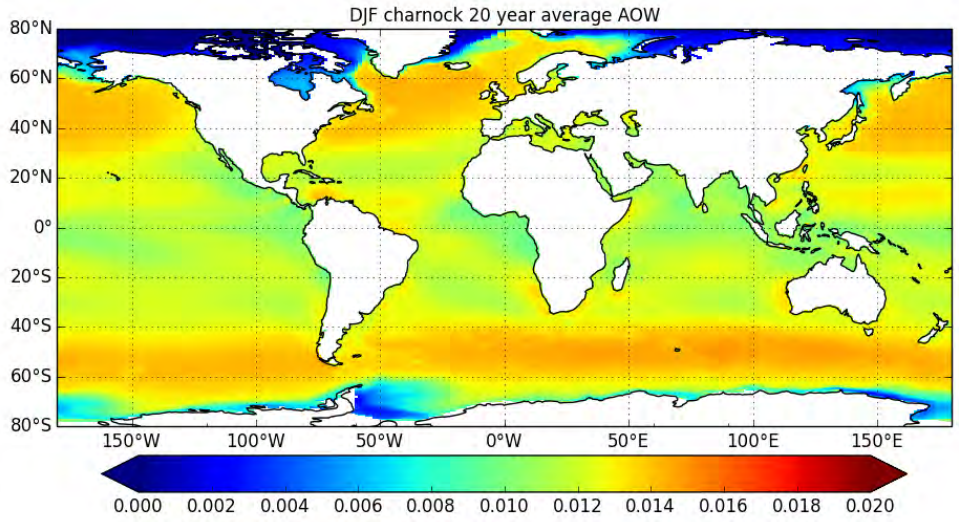

b)

Figure 4.1 The average a) JJA and b) DLF seasonal Charnock values for AOW

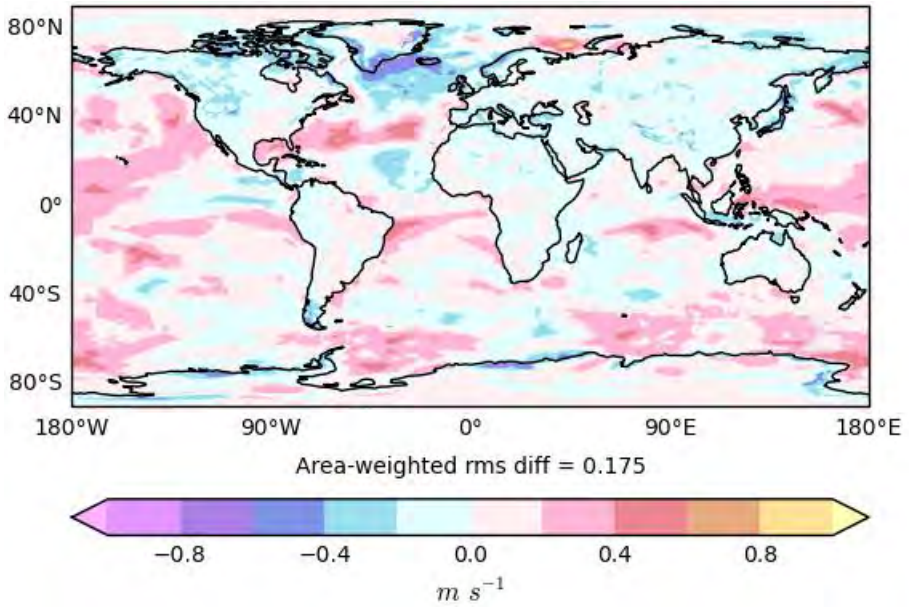

Figure 4.2 DJF 10m Scalar winds difference AOW – AO

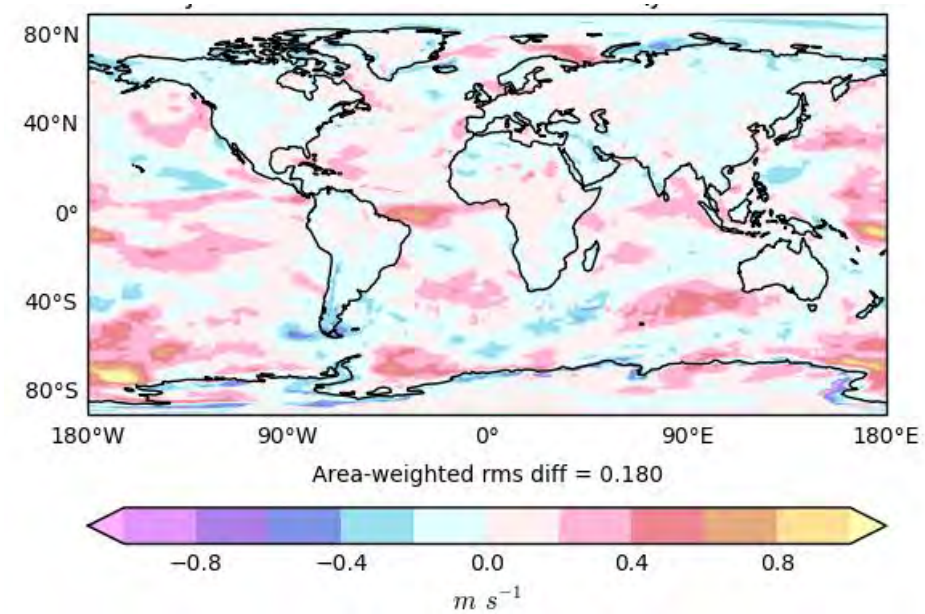

Figure 4.3 JJA 10m Scalar winds difference AOW – AO

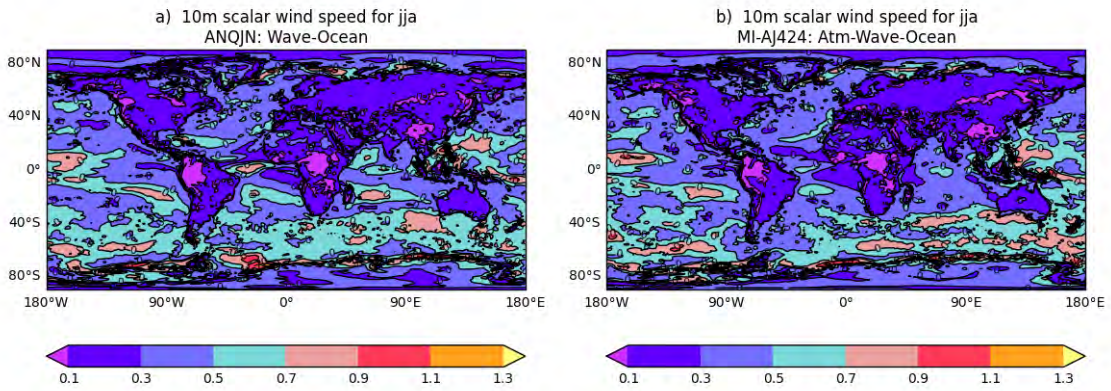

Figure 4.4 JJA Standard deviation (annual means) for 10m scalar wind speeds a) AO b) AOW

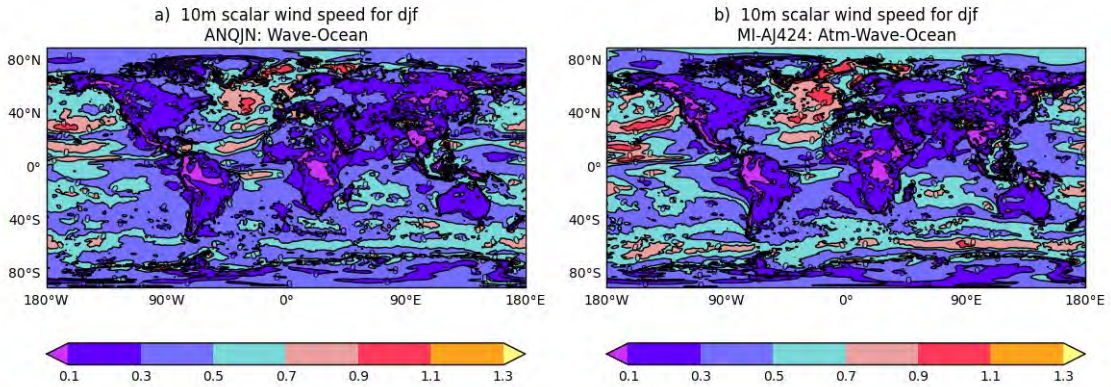

Figure 4.5 DJF Standard deviation (annual means) for 10m scalar wind speeds a) AO b) AOW

The largest local impact on the ocean of the changes in the scalar winds in AOW is seen in the North Atlantic DJF season (see figure 4.2). There is a substantial increase in the mixed layer depth in North Atlantic, in the same region that the wind speed has increased (figure 4.7). Some increases in the mixed layer depth can be seen globally where the wind speed is increased in figure 4.7, however the largest increase occurs in the North Atlantic. This increase in the wind speed did not occur in AW-ST4 in this part of the North Atlantic and suggests that further feedback is occurring from the ocean around the region of the Gulf Stream. A small increase in precipitation also occurs in this region, which is consistent with the increase in precipitation and wind speed seen in the AW-ST4 experiment (figure 4.6b).

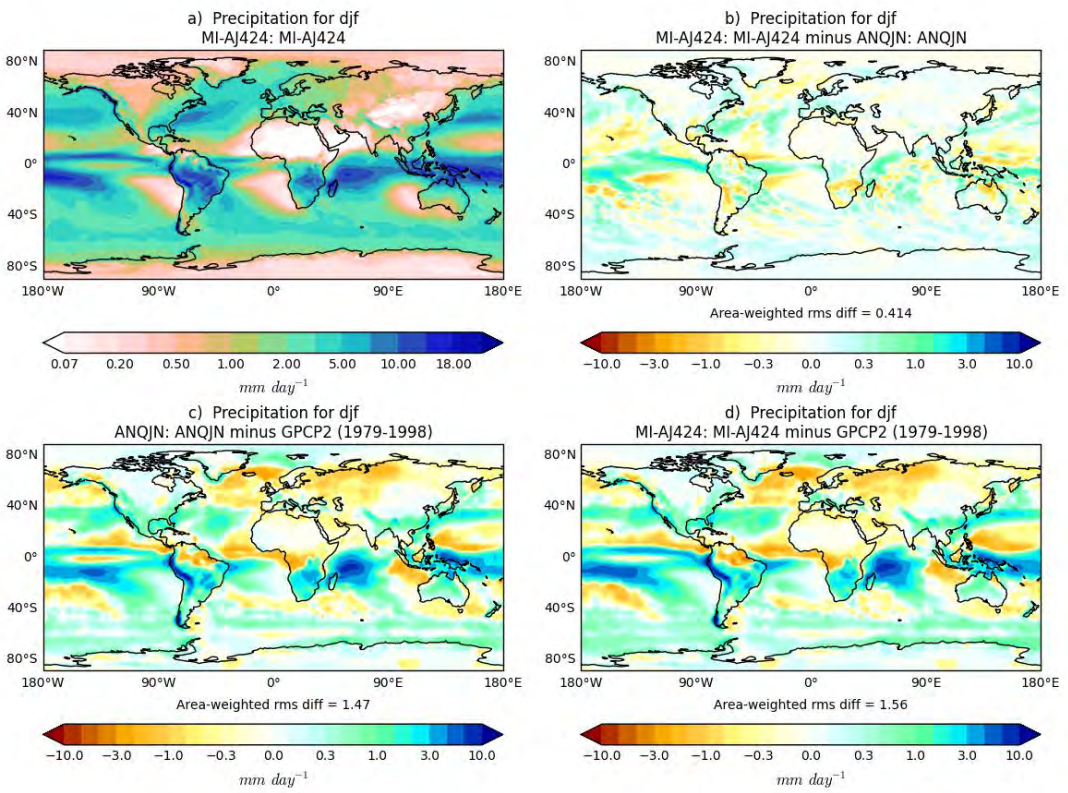

Figure 4.6 Precipitation changes for AOW in DJF a) Precipitation, b) Difference AOW -AO, c) Bias AO d) Bias AOW

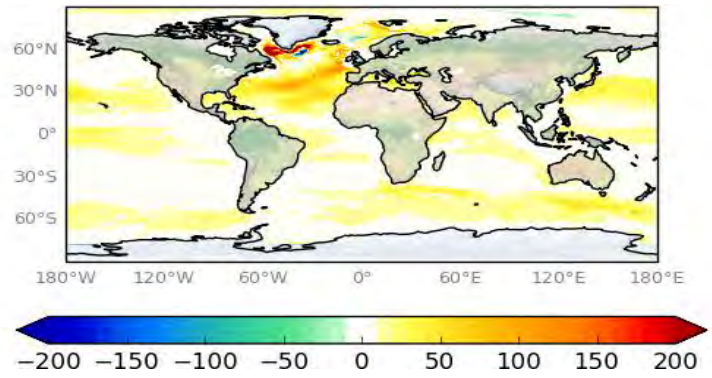

Figure 4.7 DJF Mixed layer difference AOW - AO

4.2 Sea Surface Temperature and salinity

The seasonal mean differences in Sea Surface Temperature (SST) between the wave-atmosphere-ocean experiment and the control are shown in figures 4.8 and 4.9. Globally there is a slight increase in the SST. In DJF (figure 4.8), SST is increased in the equatorial regions and in part of the Southern Ocean by approximately 1°C. In the mid-

latitudes it is largely unchanged and in parts of the Northern Hemisphere there is a decrease of about 1°C. This decrease is most significant in the North Atlantic, particularly around the Gulf Stream. In JJA the pattern of change is different (figure 4.9); the increase in SST does not appear to be confined to any particular latitudes and occurs in parts of all the main ocean basins. There is still a small area of colder water around the region of the Gulf Stream however. The reason for these changes is not clear; it is possible that changes in surface stress and precipitation have modified the evaporation which in turn causes changes to the atmospheric budget. There are some changes to the total precipitation and evaporation of 0.03mm/day in the AOW compared to the AO run. A larger change over the ocean occurs, with an increase of 0.05mm/day. This suggests that the change in the Charnock parameter may be affecting the evaporation over the ocean. The atmosphere also had an increase in the total water vapour which could be causing a slightly warmer climate.

In order to try and understand the significance of the changes in the SST the results of the AOW were compared with a different time period of the AO run (2000-2018), the annual difference is shown in figure 4.10. Comparison with a different time period of the control run shows no systematic increase in the SST between the two runs. It is interesting that the North Atlantic is about a degree cooler in this case. Figure 4.11 also shows the time series of the global sea surface temperature for AOW and AO. There is a continued upward trend in the SST of both runs; however the temperature difference between the two runs appears to be decreasing over time. The changes that were seen in the SST are however fairly typical of the changes that are seen in coupled climate models that are unconstrained.

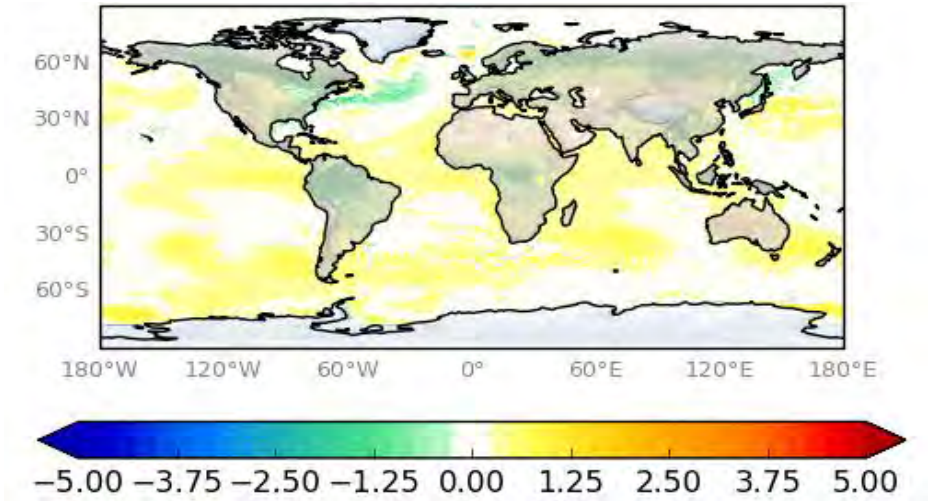

Figure 4.8 DJF SST difference AOW - AO

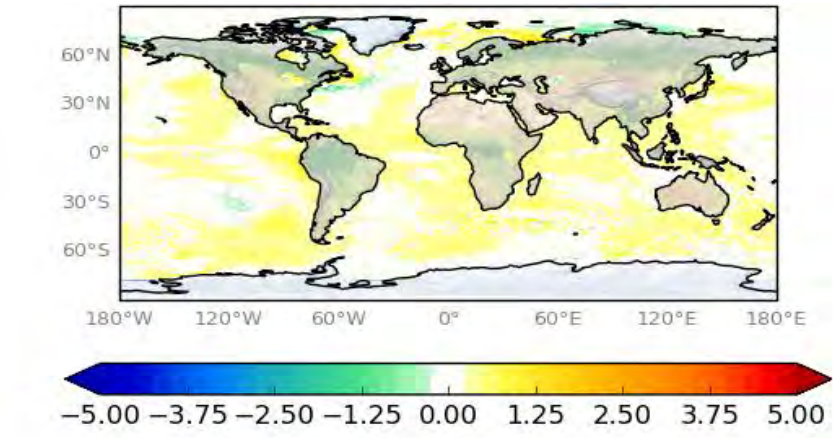

Figure 4.9 JJA SST difference AOW – AO

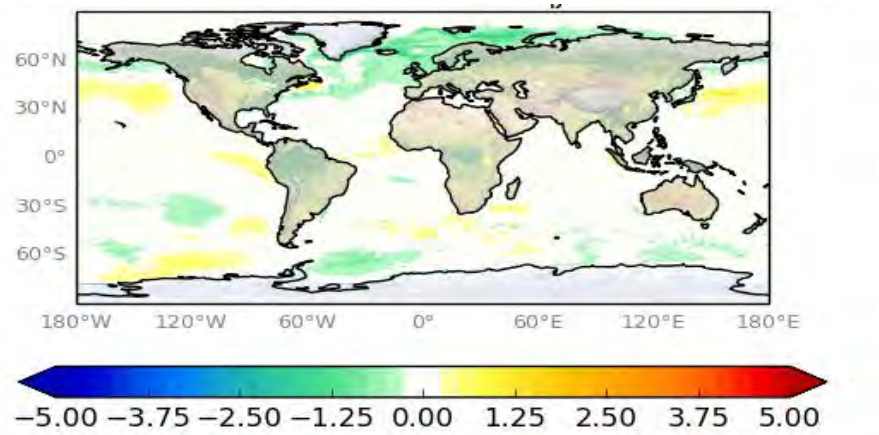

Figure 4.10 Annual SST difference AOW (1989-2007) – AO (2000-2018)

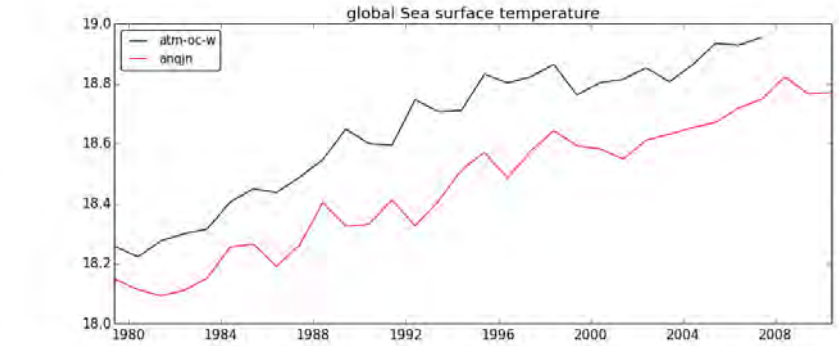

Figure 4.11 Annual global SST timeseries; red shows AO and black AOW

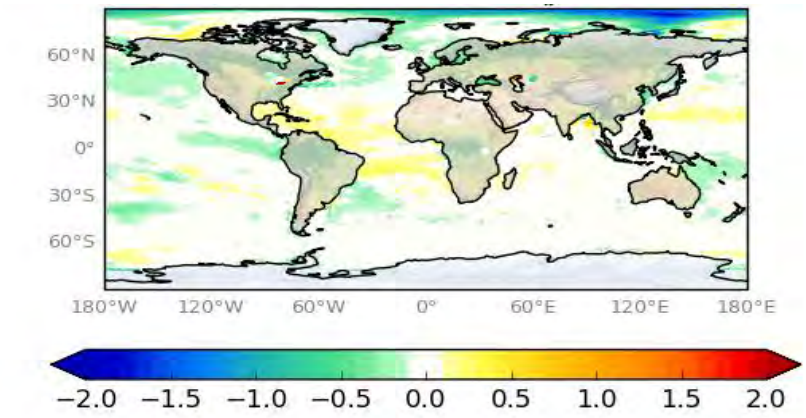

Figure 4.12 Annual SSS difference AOW - AO

The annual mean difference in sea surface salinity (SSS) between AOW and the control is shown in figure 4.12. There is almost no change in the Southern Ocean storm belt region. There is an increase of about 0.3 psu in some equatorial regions such as the Atlantic and the eastern equatorial Pacific. Most of the central South Atlantic has an increase in the SSS, while the North Atlantic, particularly around the Gulf Stream contains fresher water; this corresponds to an increase in precipitation in this region. There is an area of fresher water stretching from South America into the western equatorial pacific. This area is also associated with a seasonal increase in the total column water vapour and increased precipitation (figure 4.6 b).

4.3 Heat Fluxes

In general the global sensible heat and latent heat fluxes were not significantly affected by the wave coupling, however there is some sensitivity again around the region of the Gulf Stream, these are shown in figures 4.13 and 4.14 as difference plots. The decrease in the latent heat flux around the Gulf Stream appears to be consistent with the decrease in the SST that occurs in this region in AOW. The global fluxes over the ocean had some changes, overall the net surface heat flux over the ocean was increased in AOW, while changes over the land where much smaller. A summary of the global budgets is shown in table 2. There was also some variability in the case of the atmosphere-wave only experiments, these are summarised in table 3.

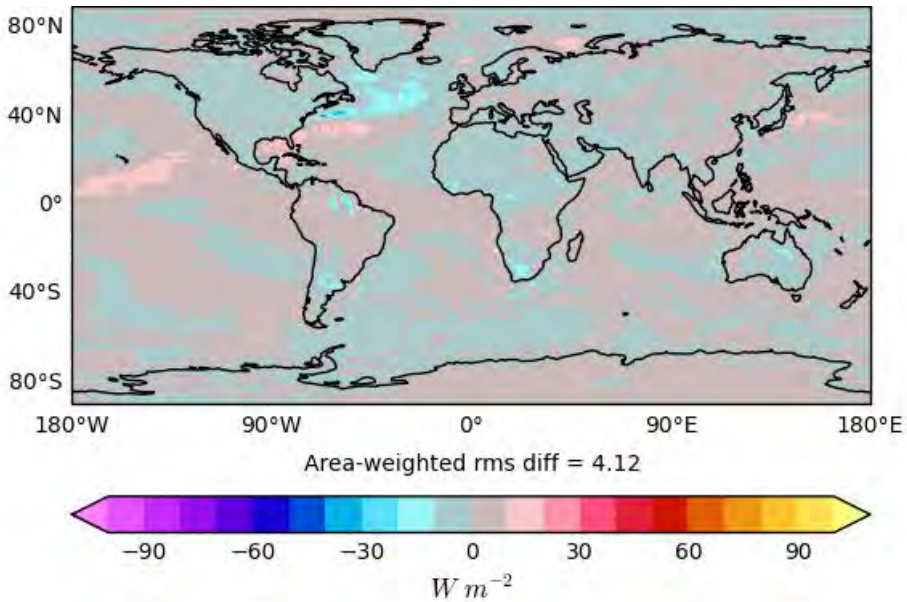

Figure 4.13 DJF Latent heat flux difference AOW – AO

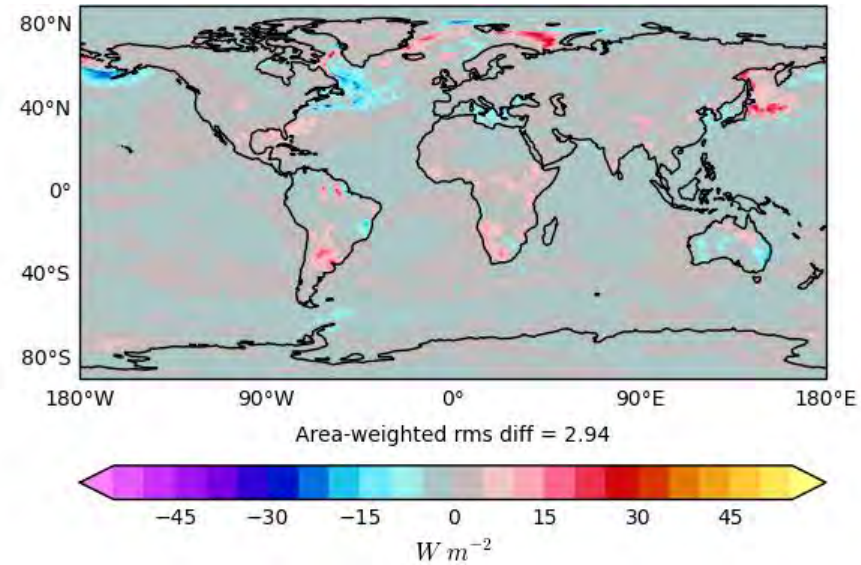

Figure 4.14 DJF Sensible heat flux difference AOW - AO

Table 2 Summary of budget over the global ocean for AOW and AO

Description	Experiment: AOW	Control: AO
PRECIP - EVAPORATION MM/DAY	-0.3409	0.03383
NET SURFACE FLUX INTO THE ATMOSPHERE	-12.24	-11.80
NET TOA FLUX INTO THE ATMOSPHERE	11.12	10.46
NET ENERGY FLUX INTO ATMOSPHERE	-1.1283	-1.3407
NET SURFACE HEAT FLUX = LW+SW-SH-LH-SM*	2.89	2.55

*Long Wave (LW), Short Wave (SW), Sensible Heat (SH), Latent Heat (LH), Snow Melt (SM).

Table 3 Summary of budget over the global ocean for AW-ST4 , AW-ST3 and U-ATM

Description	Experiment: AW-ST4	Experiment: AW-ST3	Control: U-ATM
PRECIP - EVAPORATION MM/DAY	-0.3309	-0.3299	-0.3319
NET SURFACE FLUX INTO THE ATMOSPHERE	-10.35	-10.50	-10.40
NET TOA FLUX INTO THE ATMOSPHERE	9.45	9.67	9.38
NET ENERGY FLUX INTO ATMOSPHERE	-0.8978	-0.8378	-1.0212
NET SURFACE HEAT FLUX = LW+SW-SH-LH-SM	1.58	1.77	1.61

5. Discussion

5.1 ST3 and ST4 source terms

Sensitivity studies have shown that on a decadal scale the climate of the atmosphere and ocean show some sensitivity to a sea state dependent Charnock parameter. Different wave model source terms result in different Charnock values and different global variability of the parameter. This appears to be due to the different input source term values (S_{in}), which will result in a different wave-side stress value. The ST4 source term has a sheltering parameter which results in an adhoc reduction to U^* and wind energy input to the higher frequencies. This is to balance the saturation based dissipation part of the source term. The S_{in} and S_{dis} terms are therefore generally smaller for the ST4 parameterisations than for those used in ST3. However, in the experiments here this did not translate into larger mean Charnock parameter values for the ST3 runs, since the tuning used by Bidlot (2012) for ST3 is based on a significantly lower minimum Charnock value than was used in the ST4 run and the distribution of Charnock values is governed by more frequently occurring low wind events.

The ST3 source term caused an increased positive bias in the southern hemisphere winds in the DJF season, while there was a decrease in the wind speed in some areas of the North Atlantic. In the northern hemisphere during JJA there was an increased positive bias in the scalar wind speed and also an increase in the positive bias of the winds in parts of the Southern Ocean storm belt region. This is due to the lower value of the variable Charnock parameter when ST3 is used. This has the effect of decreasing the surface drag compared to constant value of 0.018 that is used in an uncoupled atmosphere model.

The ST4 source term results in a wave spectrum that develops more slowly, with a smaller S_{in} source term; this would result in a smaller value of the Charnock parameter than the ST3 term, however the $\hat{\alpha}$ value is larger than ST3 which leads to larger Charnock values. The Charnock values are generally more variable with the ST3 source term than ST4. In some regions the seasonal average Charnock value for ST4 is close to the constant value (0.018) that is used by the uncoupled atmosphere model. In the AW-ST4 experiments the wind speed was often reduced around coastal and fetch limited areas. The North Atlantic DJF seasonal mean wind speeds were particularly sensitive to coupling using the ST4 physics. Parts of the North Atlantic saw a significant decrease in scalar wind speed; in particular the northeast Atlantic and the Labrador Sea

area were affected. These are regions where the fetch is limited and 'younger' wind-seas are more frequent; in comparison to the Pacific and Southern Ocean with more swell dominated sea-states, where increases in the scalar wind speed occurred. Changes in the scalar wind speeds were not larger than the typical errors in wind speed seen in the control model; they were also not larger than the standard deviation of the control model.

5.2 Regional sensitivity

The overall picture in the North Atlantic is not simple. On the east coast of the USA in areas of storm genesis there is an increase in the wind speed; there is also a slight increase in the storm genesis density in this region. These changes are subtle but seem to suggest some feedback occurring around the region of the Gulf Stream in the atmosphere model. The storm track analysis suggests more sensitivity in this storm track region to the coupling and there may be some changes in the divergence and convergence of winds around the Gulf Stream. The North Atlantic is an area with some of the largest variability in scalar wind speeds compared to other oceans in DJF. Many of the ocean feed backs also showed the greatest differences in the North Atlantic. The North Atlantic and in particular the subpolar region of the North Atlantic, is often shown to have a different response in climate models, this is thought to be due to changes in the Atlantic meridional overturning circulation (AMOC) (Menary and Wood 2017 – in prep). The Gulf Stream, which is essentially the upper limb of the AMOC, has been shown affect the entire troposphere (Minobe et al., 2008). This region is important for weather prediction in the UK and it is therefore an area of particular interest to the Met Office. Further work with a higher resolution model to better understand the effects of the coupling on storm genesis and evolution in this region is recommended.

5.3 Sensitivities of ocean feedbacks to atmosphere-wave coupling.

The AOW experiment had higher Charnock values than AW-ST4, particularly in the storm belt regions. There were also some differences in the global pattern of values; while the overall distribution was similar there were areas of higher values in the Indian Ocean in AOW. The scalar wind speeds were also faster in the AOW experiment compared to AW-ST4, the value of the Charnock is expected to increase in higher wind

conditions. There was an increase in the wind speed in both the North Atlantic and the Indian Ocean in AOW in DJF.

As in the AW-ST4 experiment, with AOW there is some increased sensitivity around the Gulf Stream and main North Atlantic storm track region. The intensity of the storm track is decreased in the AOW compared to the AO (control), especially in the northeast Atlantic region. The overall intensity of the winter storms is reduced. This can be explained by the response of the ocean to the coupling in these two different regions. In the main storm track area, the increased roughness from the waves increases the Charnock parameter and therefore the drag coefficient in the atmosphere model. This will in turn reduce the wind speed and slow the evolution of a storm.

The coupling of an atmosphere-wave configuration to the global ocean model introduces further sensitivities and feedbacks to the response of the atmosphere model. There are changes to the SST, which have been noted. The overall increase in the SST suggests increased ocean heat content in the AOW experiment. When the AOW experiment was compared to a different time period of the AO model run (a different 20 year period), in order to get an idea of decadal variability, the differences in the SST were much smaller. The differences seen in this study may be within the natural variability of the ocean model; however this is not clear and should be investigated further. Also of some concern is the continuing increase in the SST of the ocean, although this also occurs in the control experiment.

There is a decrease in the Sea Surface Salinity (SSS) in the North Atlantic, which is interesting given that there is actually a slight decrease in the precipitation in this region. There is an increase in precipitation south of the Gulf Stream and it is likely that this fresher water has been transported northwards. There is an increase in the SSS in the South Atlantic suggesting an increase in the difference between the physical properties of these water masses. Overall the North Atlantic is fresher and colder while the South Atlantic has become warmer and more saline. The cause of this change is not entirely clear and further studies in this region could be useful. Possibly the largest sensitivity in the ocean model occurs in the North Atlantic just south of the main storm track region in the DJF season. There is a substantial increase in the mixed layer depth in this region, which coincides with an increase in the surface wind speed. This increase in the surface wind is not seen in the AW-ST4 (wave-atmosphere only) experiment.

5.4 Performance of the atmosphere-wave coupled models.

Although this study has focussed largely in the sensitivities and differences between the experiments it is possible to give some indication of the performance of the models. The different experiments were compared against observed climatologies for the same time period. This is to give some indication of how well the wave coupled climate runs compared with the controls. In general many of the differences were small. However in some regions significant changes to the model error occurred in the wind fields.

In the AW-ST4 run there was a negative bias in the scalar wind speed created in the North East Atlantic during DJF that was not present in ATM. There was also an increased negative bias in the central Atlantic. Otherwise there were not large changes in the wind speed errors. There were some increases the positive bias in wind speeds in the Southern Ocean during DJF that occur in the control and some reduction in the positive wind speed bias around the west coast of North America. During JJA the small negative wind speed bias that occurred in the North Atlantic in ATM became a small positive bias in AW-ST4; the errors for AW-ST4 are shown in figures 3.16 and 3.17 (figures for control are in appendix 8.12a and 8.13a) In the AW-ST4 there was decrease in the latent and sensible heat fluxes in parts of the North Atlantic due to the wave coupling. This led to some improvement of a positive bias in the latent heat flux in ATM in this region during DJF. There was an increased negative sensible heat bias in the Labrador Sea (figures 8.14 and 8.15 of the appendices).

The AOW experiment wind speed changes differed from AW-ST3 and AW-ST4 experiments. In DJF the wind speed bias changes were small. There was an increase in the positive bias in wind speeds in parts of the North Atlantic. There was also a decrease in the negative bias in wind speeds in the west equatorial Pacific that occurred in AO. The increased wind speeds in the North Atlantic appear to have caused an increase in the mixed layer depth in the AOW experiment. This increase has led to an increase in the error that occurs for the mixed layer depth in the ocean model.

In JJA there were some changes in the wind speed biases in the Southern Ocean in the AOW experiment, however this is an area of high wind speeds and in general model errors are variable.

The AOW experiment also had some changes to the latent and sensible heat flux during DJF in the North Atlantic. This decrease in the latent heat flux was a small improvement in the North East Atlantic compared to the observed climatology. The decrease in the sensible heat flux around the subpolar Atlantic and Labrador Sea is an increase in the negative bias that occurs in AO. However there is some improvement in the North East Atlantic.

Overall there were some changes in the wave-coupled models that may have lead to some improvements in the climate models in certain regions. However there are also negative changes, especially in the North Atlantic storm belt regionThe reduction in the average Charnock value in all the experiments is a significant departure from the value of 0.018 that is currently used in the UM model. It is therefore unsurprising that the results of these experiments have not shown consistent results. Many of the differences in the heat fluxes and feedbacks between the controls and the experiments are within the expected variability of a 20 year climate run. The changes in the wind speed are however consistent with a reduced Charnock parameter. Due to the systematic differences found in this study, it is not clear from these results if a variable Charnock parameter from a wave model is able to add value to the atmosphere model within a coupled system without re-evaluating other parts of the parameterisations used in the representation of atmosphere-ocean momentum exchange.

6. Conclusions

6.1 Summary and Conclusions

Climate runs have been useful in establishing the sensitivity of the atmosphere and coupled atmosphere-ocean models to additional wave coupling via a variable Charnock field. There are clear sensitivities to the scalar wind speed and the wind stress as a result of the wave coupling. The largest changes are seen in the storm belt regions, but the equatorial regions are also affected. The different wave model source terms calculate a different wave induced stress for the same wind conditions due to the different Sin values for ST4 and ST3. The different source terms also have a different minimum value for the Charnock parameter which leads to different values where wind speeds are low, such as the equatorial regions. It also results in generally higher and less variable Charnock values for the ST4 source terms than the ST3.

The AW-ST4 and the AOW experiments show quite different responses to the atmosphere-wave coupling. This is due to the strength of the feedbacks from the ocean on the atmosphere. The relative wind speed due to the presence of ocean currents are accounted for in the AOW experiment and this will affect some of the changes to the wind speed. There were also some changes to the evaporation which could have been influenced by the surface roughness. This in turn has influenced the precipitation in some areas. Areas with strong ocean currents such as the Gulf Stream in the North Atlantic have also shown a different response to the coupling.

In conclusion, although the most significant sensitivities were seen in the wind speeds and the wind stress, the wave coupling via a Charnock parameter did cause changes throughout the atmosphere column. This was also seen in the ECMWF results. Not all changes were positive however. The changes in the wind speed were an improvement in some areas for example the western Pacific and some parts of the Southern Ocean. In general the same improvement in the wind speed statics that was seen in the ECMWF experiments did not occur with the UM model. In DJF the reduction in wind speed created a negative bias in the North Atlantic.

6.2 Recommendations for future work

This study has only considered the effect of the waves on the momentum transfer between the ocean surface and the atmosphere. To further understand the effect of waves on the ocean-atmosphere system, it would be useful to couple the wave and ocean model. The momentum transfer from the waves to the ocean is an important part of the system and this would in theory 'close' the momentum transfer in the AOW experiment.

It is not clear from the results of this study what the effects of the variable Charnock field may be on the atmospheric forecast, during the evolution of an individual storm. It is also not been possible to establish from this study if a variable Charnock field would provide useful information and improve the performance of the atmosphere model in these circumstances. Shorter forecast runs with data assimilation, particularly in the areas that shown the greatest sensitivity, such as the North Atlantic, to the coupling would be useful to help establish if there is added value to the models from this wave coupling approach.

7 References and Acknowledgements

7.1 Acknowledgements

Thanks to Dan Copsey,Daley Calvert and Tim Graham for their assistance in the production of the plots in this report.

7.1 References

Ardhuin, F., F. Collard, B. Chapron, P. Queffeulou, J-F. Filipot, and M. Hamon, 2008a: Spectral wave dissipation based on observations: a global validation. Proc. Chinese–German Joint Symp. on Hydraulics and Ocean Engineering, Darmstadt, Germany, Technische Universitat Darmstadt, 391–400. [Available online at http://www.comc.ncku.edu.tw/joint/joint2008/papers/69.pdf].

Ardhuin, F., B. Chapron and F. Collard, 2009a: Ocean swell evolution from distant storms. Geophys. Res. Lett., 36, L06607.

Ardhuin F. . Mari ę N. Rascle, P. Forget and A. Roland, 2009b: Observation and estimation of Lagrangian, Stokes and Eulerian currents induced by wind and waves at the sea surface. J. Phys. Oceanogr., 39(11), 2,820– 2,838.

Ardhuin, F., W. E. Rogers, A. V. Babanin, J. Filipot, R. Magne, A. Roland, A. van der Westhuysen, P. Queffeulou, J. Lefevre, L. Aouf and F. Collard, 2010: Semiempirical dissipation source functions for ocean waves. Part I: Definition, calibration, and validation. J. Phys. Oceanogr., 40, 1,917– 1,941.

Bidlot, J.-R., 2012: Present status of wave forecasting at E.C.M.W.F. in Proceedings of ECMWF workshop on ocean wave forecasting, June.

Babanin, A. V., and I. R. Young, 2005: Two-phase behaviour of the spectral dissipation of wind waves. Proc. Fifth Int. Symp. Ocean Wave Measurement and Analysis, Madrid, Spain, ASCE, Paper 51

Banner, M. L., A. V. Babanin, and I. R. Young, 2000: Breaking probability for dominant waves on the sea surface. J. Phys. Oceanogr., 30, 3145–3160.

Breivik, Ø., Mogensen, K., Bidlot, J.R., Balmaseda, M.A. and Janssen, P.A., 2015. Surface wave effects in the NEMO ocean model: Forced and coupled experiments. Journal of Geophysical Research: Oceans, 120(4), pp.2973-2992.

Cavaleri, L., Fox-Kemper, B. and Hemer, M., 2012. Wind waves in the coupled climate system. Bulletin of the American Meteorological Society, 93(11), pp.1651-1661.

Charnock, H., 1955: Wind stress on a water surface. Quart. J. Roy. Meteor. Soc., 81, 639–640.

Chelton, D. B., and S.-P. Xie (2010), Coupled ocean-atmosphere interaction at oceanic mesoscales, Oceanography, 23(4), 52–69.

Drennan, W.M., Graber, H.C., Hauser, D. and Quentin, C., 2003. On the wave age dependence of wind stress over pure wind seas. Journal of Geophysical Research: Oceans, 108(C3).

Gaspar, P., Grégoris, Y. and Lefevre, J.M., 1990. A simple eddy kinetic energy model for simulations of the oceanic vertical mixing: Tests at station Papa and Long-Term Upper Ocean Study site. Journal of Geophysical Research: Oceans, 95(C9), pp.16179-16193.

Hasselmann, S., and K. Hasselmann, 1985. "Computations and parameterizations of the nonlinear energy transfer in a gravity-wave spectrum. Part I: A new method for efficient computations of the exact nonlinear transfer integral." Journal of Physical Oceanography 15.11 : 1369-1377.

Komen, G. J., K. Hasselmann, and S. Hasselmann, 1984: On the existence of a fully developed windsea spectrum. J. Phys. Oceanogr., 14, 1271–1285.

Janssen, P. A. E. M., 1982: Quasilinear approximation for the spectrum of wind-generated water waves. J. Fluid Mech., 117, 493–506.

Janssen, P. A. E. M., 1989: Wind-induced stress and the drag of air-flow over sea waves. J. Phys. Oceanogr., 19, 745–754.

Janssen, P. A. E. M., 1991: Quasi-linear theory of of wind wave generation applied to wave forecasting. J. Phys. Oceanogr., 21, 1,631–1,642.

Janssen, P.A. and Viterbo, P., 1996. Ocean waves and the atmospheric climate. Journal of climate, 9(6), pp.1269-1287.

Janssen, P.A.E.M., Doyle, J.D., Bidlot, J., Hansen, B., Isaksen, L. and Viterbo, P., 2002. Impact and feedback of ocean waves on the atmosphere. Advances in Fluid Mechanics, 33, pp.155-198.

Li, J. G., 2008: Upstream nonoscillatory advection schemes. Mon. Wea. Rev., 136, 4,709–4,729.

Lock. A, Edwards. J and Boutle. I. Unified Model Documentation Paper 024 for Unified Model Version 10.8; 2017, Met Office.Madec, G., 2008. NEMO reference manual, ocean dynamic component: NEMO-OPA. Note du Pôle de modélisation, Institut Pierre Simon Laplace, France, Technical Report, 27.

Megann, A., Storkey, D., Aksenov, Y., Alderson, S., Calvert, D., Graham, T., Hyder, P., Siddorn, J. and Sinha, B., 2014. GO5. 0: The joint NERC-Met Office NEMO global ocean model for use in coupled and forced applications. Geoscientific Model Development, 7(3), pp.1069-1092.

Miles, J. W., 1957: On the generation of surface waves by shear flows. J. Fluid Mech., 3.

Minobe, S., A. Kuwano-Yoshida, N. Komori, S.-P. Xie, and R. J. Small (2008), Influence of the Gulf Stream on the troposphere, Nature, 452, doi:10.1038/nature06690.

Roberts, M. J., H. T. Hewitt, P. Hyder, D. Ferreira, S. A. Josey, M. Mizielinski, and A. Shelly (2016), Impact of ocean resolution on coupled air-sea fluxes and large-scale climate, Geophys. Res. Lett., 43, 10,430–10,438, doi:10.1002/2016GL070559.

Shimura, T., Mori, N., Takemi, T. and Mizuta, R., 2017. Long-term impacts of ocean wave-dependent roughness on global climate systems. Journal of Geophysical Research: Oceans, 122(3), pp.1995-2011.

SSMM, H., 1992. A model for the global variation in oceanic depth and heat flow with lithospheric age. Nature, 359(1).

Taylor, P.K. and Yelland, M.J., 2001. The dependence of sea surface roughness on the height and steepness of the waves. Journal of physical oceanography, 31(2), pp.572-590.

Tolman, H. L., 1991: A third-generation model for wind waves on slowly varying, unsteady and inhomogeneous depths and currents. J. Phys. Oceanogr., 21, 782–797.

Tolman, H., 2014. WAVEWATCH III Development Group. User manual and system documentation of wavewatch iii version, 4.

Williams, K. D., Harris, C. M., Bodas-Salcedo, A., Camp, J., Comer, R. E., Copsey, D., & Hyder, P. (2015). The met office global coupled model 2.0 (GC2) configuration. Geoscientific Model Development, 8(5), 1509-1524.

Wood, N., Staniforth, A., White, A., Allen, T., Diamantakis, M., Gross, M., Melvin, T., Smith, C., Vosper, S., Zerroukat, M. and Thuburn, J. (2014), An inherently mass-conserving semi-implicit semi-Lagrangian discretization of the deep-atmosphere global non-hydrostatic equations. Q.J.R. Meteorol. Soc., 140: 1505–1520. doi:10.1002/qj.2235

Young, I. R., and A. V. Babanin, 2006: Spectral distribution of energy dissipation of wind-generated waves due to dominant wave breaking. J. Phys. Oceanogr., 36, 376–394.

8 Appendix

8.1 Changes in wind stress

Changes to the wind stress largely reflect the sensitivities in the 10m scalar wind speeds. Most notably there is a reduction in the wind stress in the North Atlantic for the AW-ST3 and AW-ST4 runs. The reduction is larger for AW-ST4, which is consistent with the larger reduction in wind speeds in DJF, see figures 8.1 and 8.2.

In JJA there is an increase in the wind stress in parts of the Southern Ocean for AW-ST3 and AW-ST4. These areas also correspond to increases in the 10m wind speed (figures 8.3 and 8.4.)

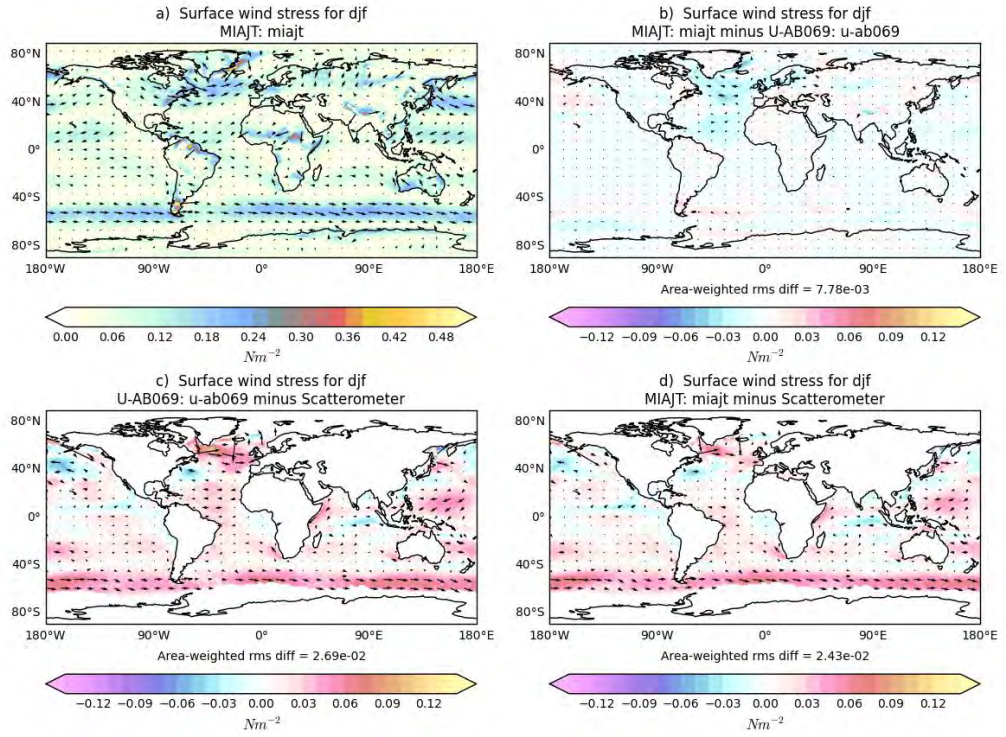

Figure 8.1 Wind stress for DJF a) AW-ST3 b) AW-ST3 – ATM c) ATM – Scatterometer d) AW-ST3 - scatterometer

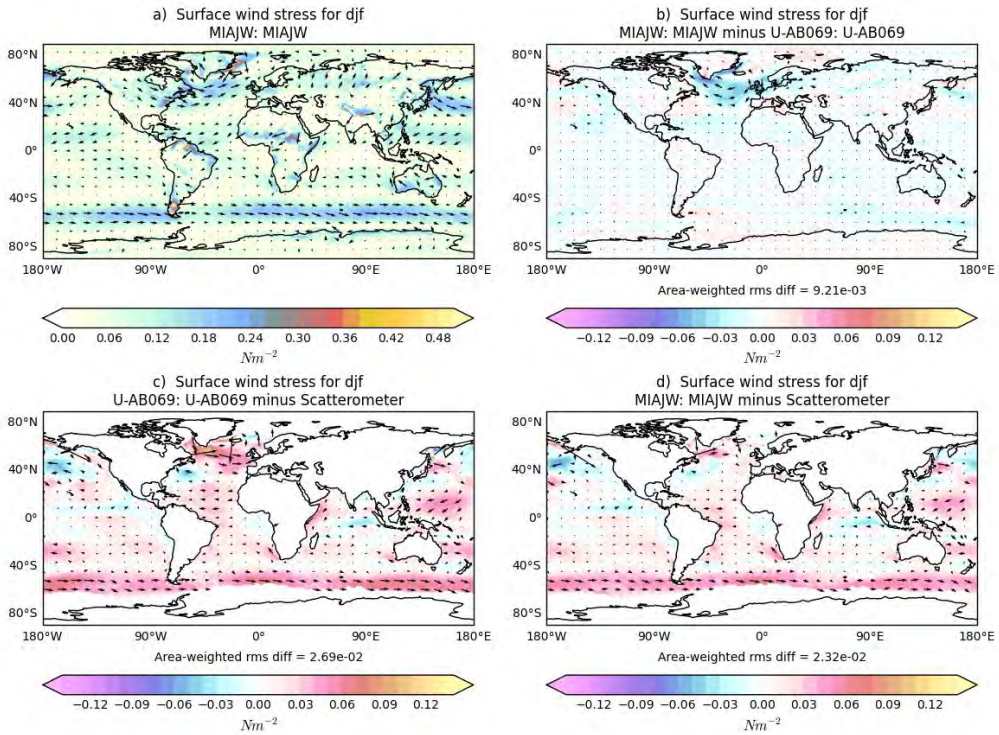

Figure 8.2 Wind stress for DJF a) AW-ST4 b) AW-ST4 – ATM c) ATM – Scatterometer d) AW-ST4 - scatterometer

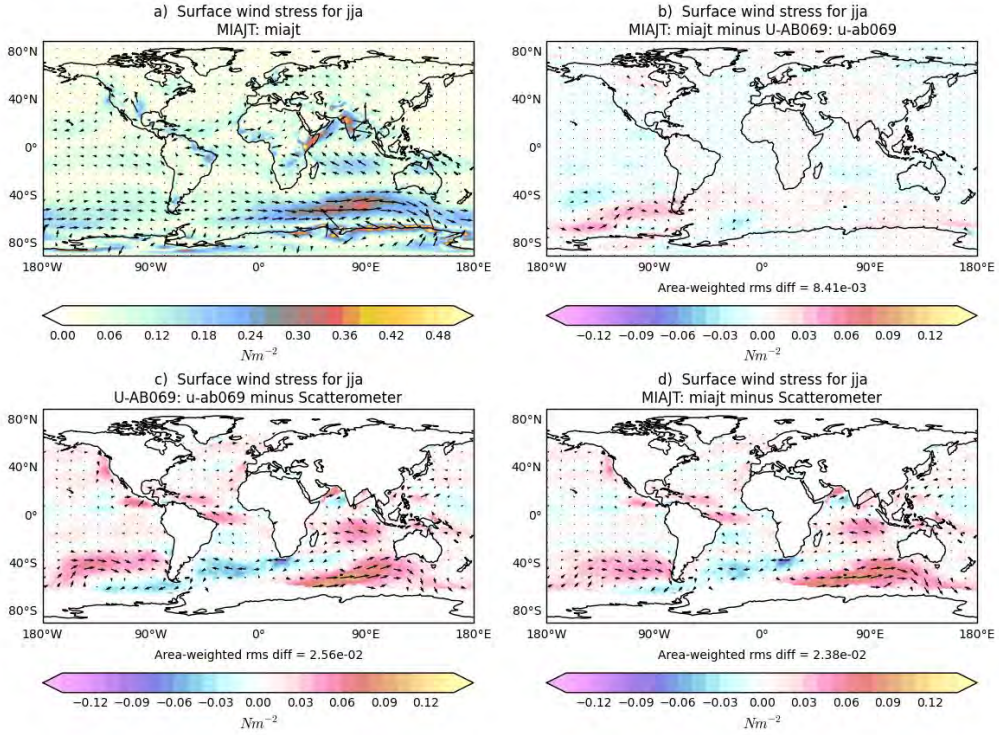

Figure 8.3 Wind stress for JJA a) AW-ST3 b) AW-ST3 – ATM c) ATM – Scatterometer d) AW-ST3 - scatterometer

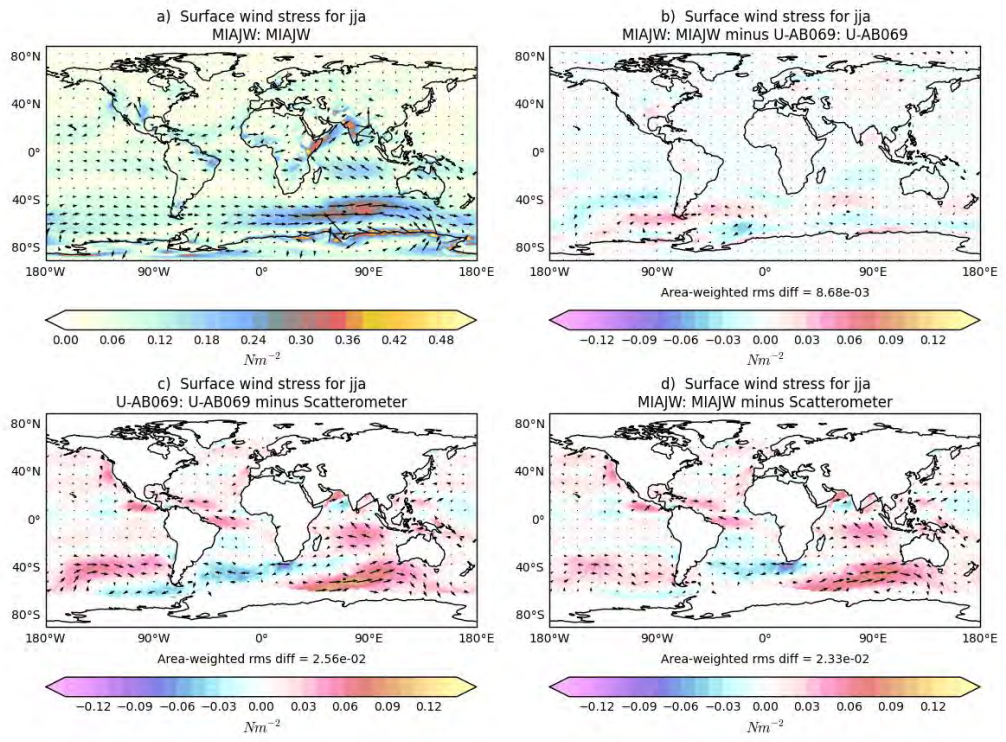

Figure 8.4 Wind stress for JJA a) AW-ST4 b) AW-ST4 – ATM c) ATM – Scatterometer d) AW-ST4 - scatterometer

8.2 Changes in Pressure at mean sea level.

The main areas of sensitivity are in the North Atlantic and the Southern Ocean during in the North Hemisphere and South Hemisphere winters respectively.

In the North Atlantic and over parts of the Arctic there is an increase in the PMSL of 2-4 hPa. This is over the area of the North Atlantic where a decrease in the scalar wind speed also occurs. In the control run there is a positive bias in this area compared to the ERA-Interim dataset; this bias is slightly increased in the coupled run (figure 8.6). These areas of decreased precipitation largely correspond to areas of decreased wind speed (figure 8.6).

In the Southern Ocean during JJA there is a decrease in the Pressure Mean Sea Level (PMSL) in two areas of the main storm belt. The positive bias in the model (compared to the ERA-Interim) present in the control at between 60º to 70º S and 90º-80º W (see figure 8.7), is improved in the wave-atmosphere coupled run. The negative bias that can be seen (figure 8.2) south of Australia is slightly increased in the coupled run compared to the control.

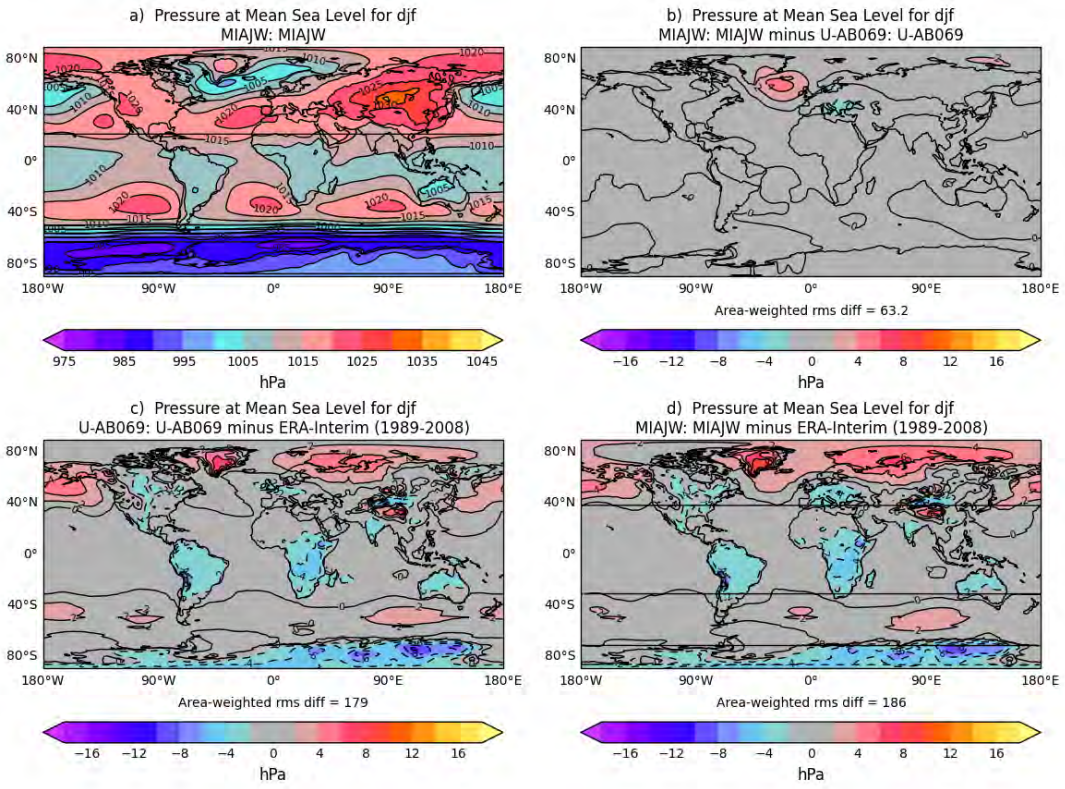

Figure 8.6 PMSL DJF a) AW-ST4 b) AW-ST4 – ATM c) ATM – ERA-Interim d) AW-ST4 – ERA-Interim

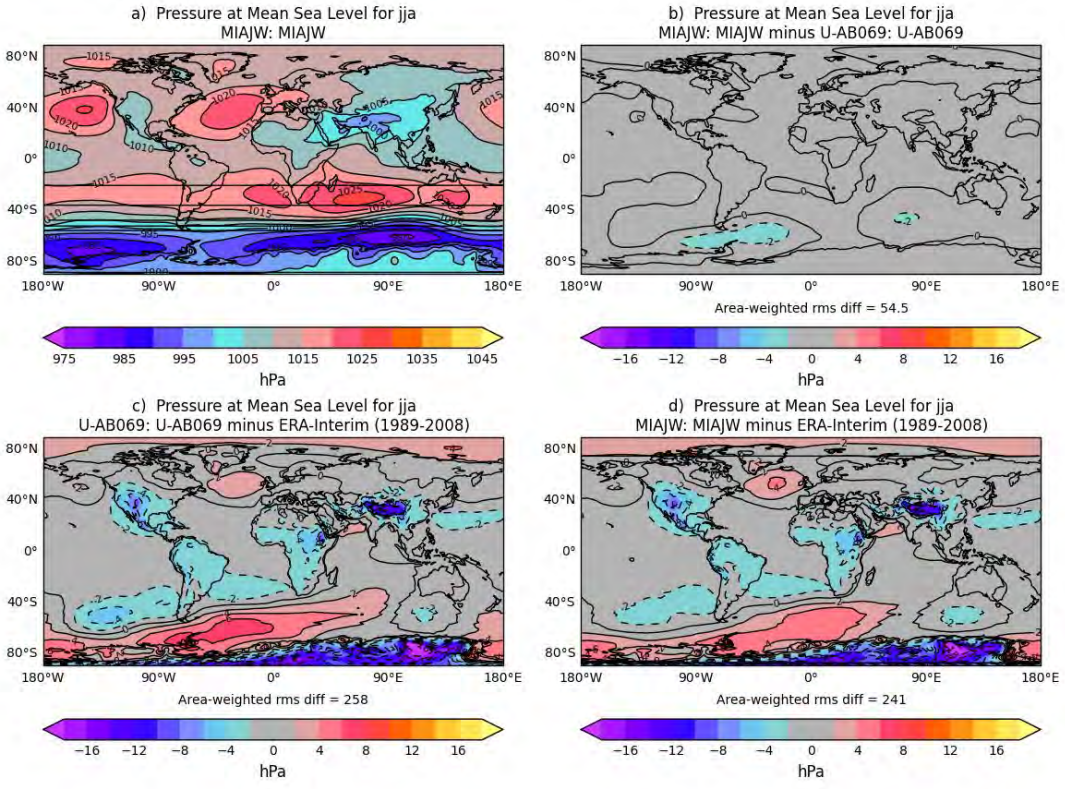

Figure 8.7 PMSL DJF a) AW-ST4 b) AW-ST4 – ATM c) ATM – ERA-Interim d) AW-ST4– ERA-Interim

8.3 Geopotential Height

Some changes in the geopotential height are evident in the storm track regions in the coupled wave-atmosphere run. A decrease of more the 40m is seen in the North Hemisphere winter (DJF) over Europe, while there is an increase to the north of the UK and over Greenland. The difference between the coupled run (AW-ST4) and the control (ATM) is shown in figure 8.8 along with the difference between both runs and the ERA-Interim dataset. There is an increase in the positive bias over Siberia and the Arctic in AW-ST4 and an increase in the negative bias over Europe. Over parts of the North Atlantic a negative bias has been replaced by a positive bias in the 500mb height, suggesting a shifting of the main storm track in AW-ST4. In the southern hemisphere there is a decrease of about 20m in some areas. It is not clear whether or not this is an improvement.

In the South Hemisphere winter (JJA) there is relatively little change in the 500m height in the North Hemisphere. There is however some increase in the 500mb over the North Atlantic, this can be seen in figure 8.9. There are some changes around the Southern Ocean, which suggests that the main storm track in this region may have shifted or become more ‘wavy’ as was found by Janssen et al. (2001).

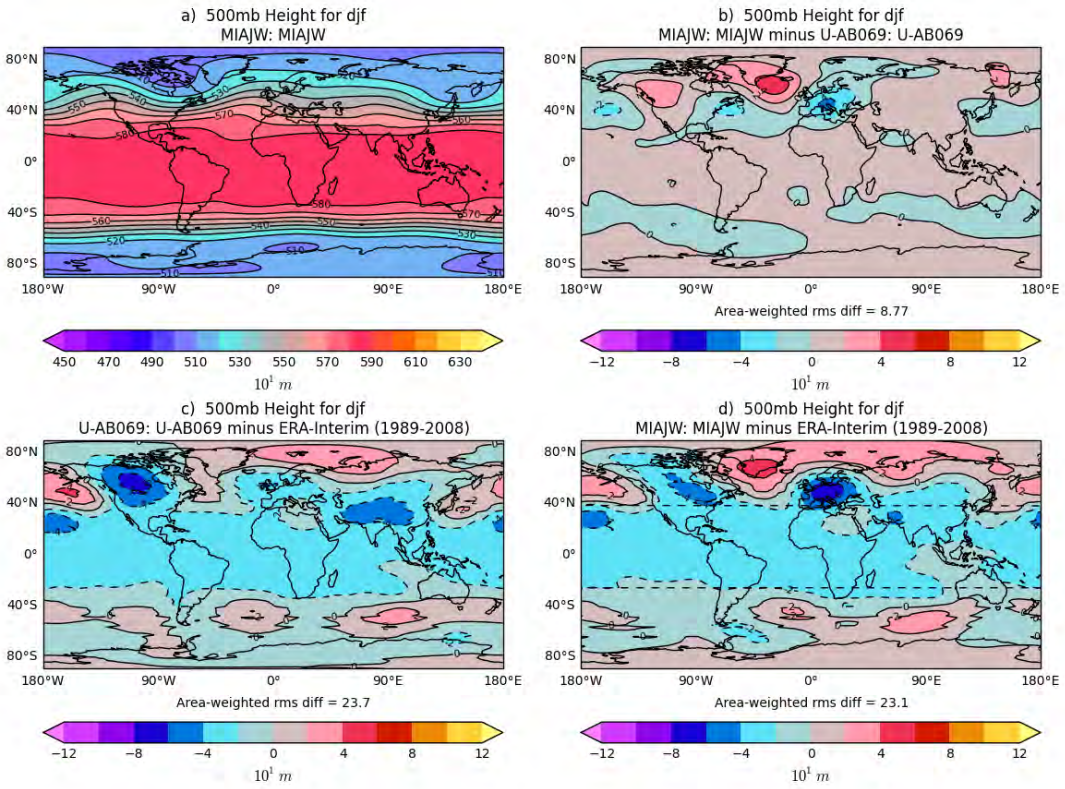

Figure 8.8 Geopotential Height DJF a) AW-ST4 b) AW-ST4 – ATM c) ATM – ERA-Interim d) AW-ST4– ERA-Interim

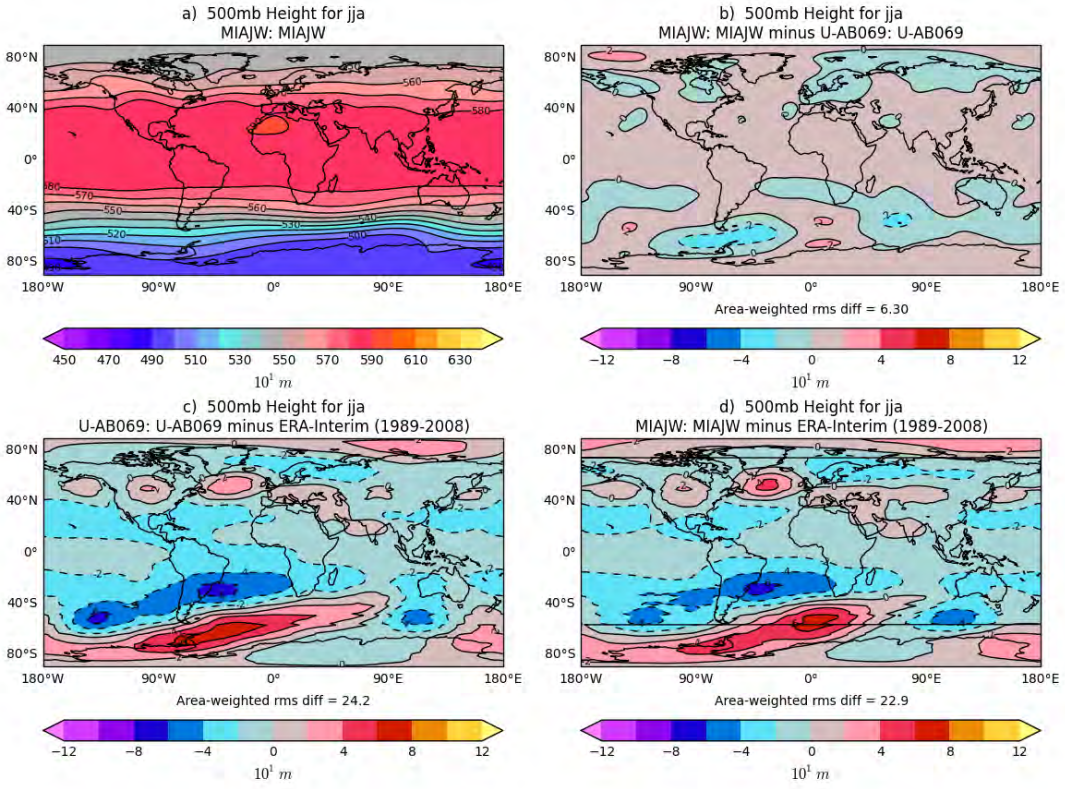

Figure 8.9 Geopotential Height JJA a) AW-ST4 b) AW-ST4 – ATM c) ATM – ERA-Interim d) AW-ST4– ERA-Interim

8.4 Wind speed errors compared to climatology

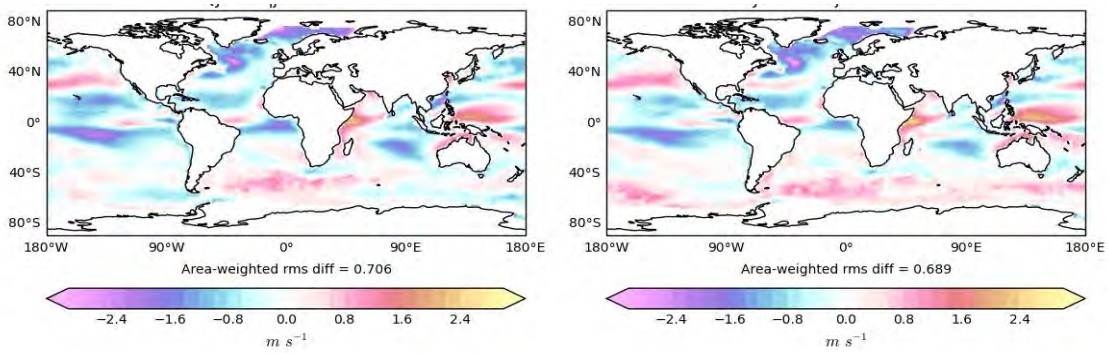

Figure 8.10 Wind speed errors for a) AO and b) AOW in JJA

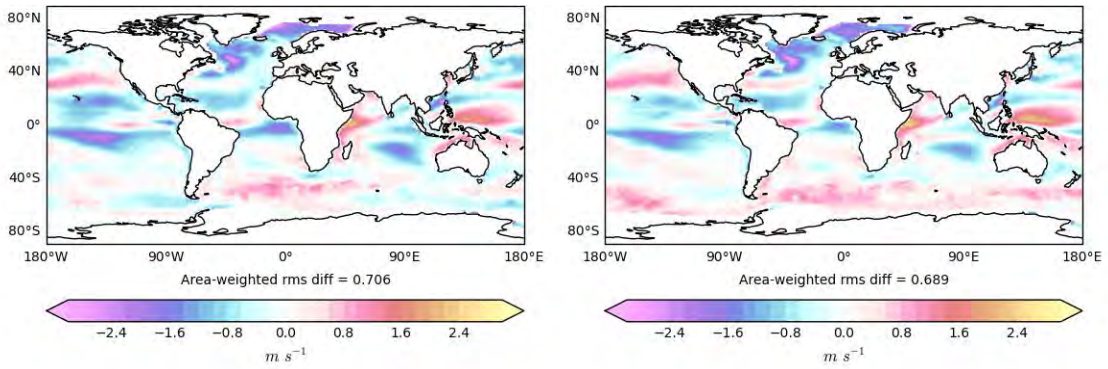

Figure 8.11 Wind speed errors for a) AO and b) AOW in DJF

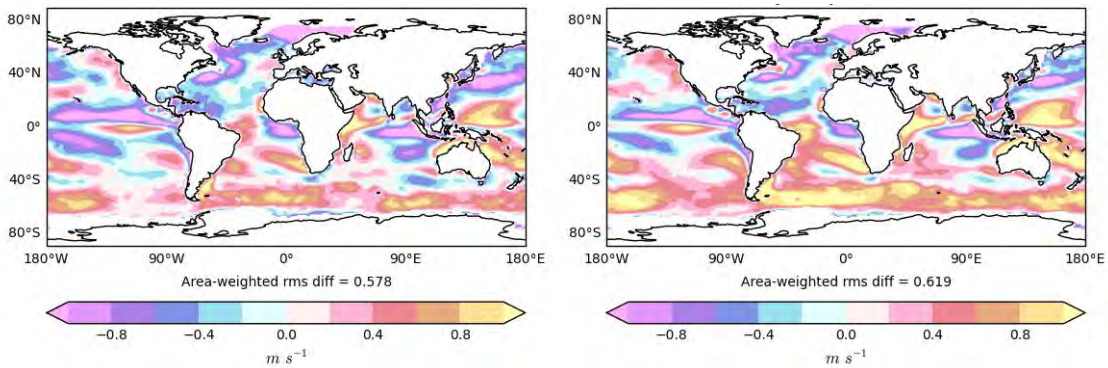

Figure 8.12 Wind speed error for a) ATM and b) AW-ST3 in DJF

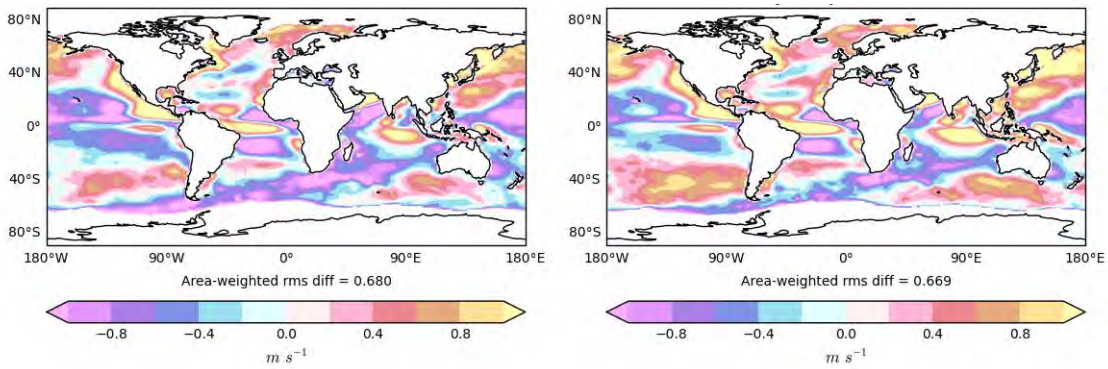

Figure 8.13 Wind speed error for a) ATM and AW-ST3 in JJA

8.5 Heat flux changes for AW-ST4

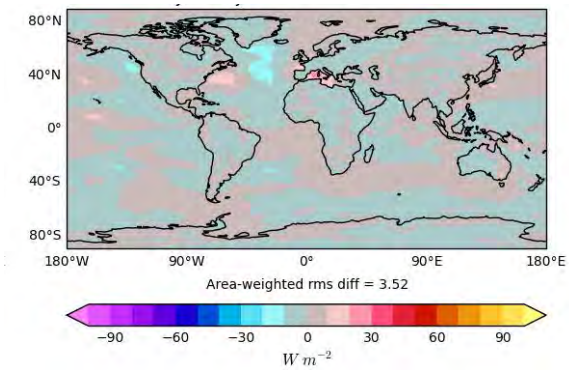

Figure 8.14 Heat flux difference AW-ST4 minus ATM in DJF

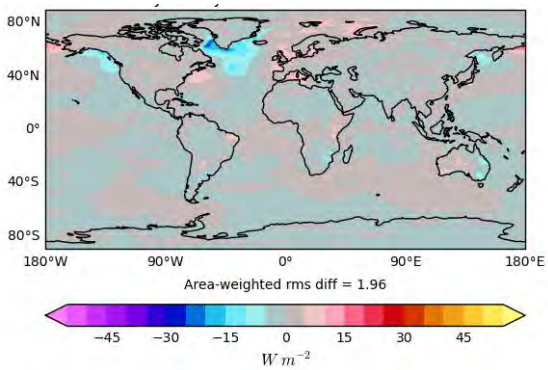

Figure 8.15 Sensible heat flux difference AW-ST4 minus ATM in DJF